M 2021

U.PORTO
FEUP FACULDADE DE ENGENHARIA
UNIVERSIDADE DO PORTO

NOVEL DIFFUSION BARRIER LAYERS FOR ADVANCED COPPER INTERCONNECT METALLIZATION

LILIANE CRISTINA GONÇALVES SAVARIS
MASTER'S DEGREE DISSERTATION OF METALURGICAL AND MATERIAL ENGINEERING AT
FACULTY OF ENGINEERING OF UNIVERSITY OF PORTO

SUPERVISOR: PROFESSOR RÚBEN SANTOS

Candidato: Liliane Cristina Gonçalves Savaris	*Código: 201601884*
Título: Novel diffusion barrier layers for advanced copper interconnect metallization	
Data: 07/10/2021	
Local: Faculdade de Engenharia da Universidade do Porto - FEUP	

Júri	*Presidente: Manuel Fernando Gonçalves Vieira*	*DEMM/FEUP*
	Arguente: João Pedro dos Santos Hall Agorreta de Alpuim	*DEF-Uminho*
	Orientador: Rúben Filipe da Silva Santos	*DEMM/FEUP*

Abstract

The semiconductor industry is in constant growth. The consumer goods in general are becoming faster, more efficient, and more sophisticated every day. A continuous exponential increase in the number of transistors in an integrated circuit allows this advance in technology. However, this means that the size of the transistors and, consequently, the size of the interconnects must be reduced, down to the nanometre scale. The reduction in size of the interconnects brought up a lot of challenges for the industry, namely the substitution of Ta/TaN for a seedless diffusion barrier, in order to allow direct Cu plating and minimize the increase in the resistivity caused by the shrinking. Direct copper plating capability and wetting ability of Ru-W diffusion barrier are investigated in this work. Seedless Cu electroplating was performed on top of Ru-W thin films with Ru/W atomic ratio close to 1. The electrodeposition process was carried out using a Cu sulphate acidic electrolyte (pH < 2). A continuous Cu film was deposited on Ru-W at average current density of 5 $mA \cdot cm^{-2}$ and above, however, the formation of large particles, with fast growing rate, prevented Cu deposition underneath them. Pulsed-reverse current with average current density of 10 5 $mA \cdot cm^{-2}$ helped reduce particle size, which could improve substrate coverage. The adhesion between Cu and Ru-W was investigated through submitting PVD-Cu/Ru-W/SiO_2/Si stacks with two different thicknesses (35 and 70 nm) to annealing treatment at different temperatures. Pinhole formation was observed for both samples, but in larger quantity for the 35 nm Cu film. These defects are attributed in the literature as the beginning of dewetting phenomena, however, since the number and/or size of the pinhole did not change with the increase of the annealing temperature, it is possible that they are a result from the PVD process, where thin films usually have discontinuities. For both thicknesses, Cu films did not present cracking and agglomeration, characteristics of the dewetting phenomena, up to 700 ºC, being the results comparable for Cu on Ta/TaN.

Key words

Copper interconnects, diffusion barrier layer, seedless electroplating, Ru-W.

Acknowledgments

I would first like to thank my supervisor, Professor Rúben Santos, whose knowledge, availability, patience and support where essential to the development of this work. Thank you for always pushing me to fill in the gaps and bring my work to a higher level.

I would like to thank Eng. Bruno M. C. Oliveira, for all the help and collaboration during the experimental procedures, as well as for the FIB images and results.

I would also like to thank Professor Filomena Viana, for arguer my Seminar work, which served as a foundation for the literature review of this work. Thank you for pointing me improvement opportunities for my work.

Finally, I would like to thank project USECoIN – Understanding the Structural Evolution of Seedless Copper Interconnects for Nanoelectronics - (PTDC/CTM-CTM/31953/2017), financed by Portugal 2020 through European Regional Development Fund (FEDER) in the frame of Operational Competitiveness and Internationalization Programme (POCI), where this work was conducted and supported.

Index

List of Figures

List of Tables

List of Abbreviations

AFM	Atomic force microscopy
ALD	Atomic layer deposition
BSE	Backscattered electrons
CVD	Chemical vapour deposition
DC	Direct-current
EDS	Energy dispersive X-ray spectroscopy
EP	Electroplated/electrodeposited
FIB	Focused ion-beam
GIXRD	Grazing incidence X-ray diffraction
IC	Integrated circuit
ITRS	International Technology Roadmap for Semiconductors
PC	Pulsed current
PECVD	Plasma enhanced chemical vapour deposition
PVD	Physical vapour deposition
PRC	Pulse-reverse current
RTA	Rapid thermal annealing
RF	Radio frequency
SEM	Scanning electron microscopy
TEM	Transmission electron microscopy
XRD	X-ray diffraction
XPS	X-ray photoelectron spectroscopy

1. Introduction

In 1965, Gordon Moore published an article predicting that the number of transistors in a chip would double every 18 months [1]. With extrapolated data, Moore was able to predict that in 1975, ten years after the article publishing date, a single chip would have 64,000 transistors. Despite it being an empirical observation, the prediction was completely accurate in 1975 and continues to be at present date. That prediction is known as the Moore's Law and became the roadmap to the semiconductor industry, allowing massive advances in computational capacity and performance. Figure 1 shows the evolution in the number of transistors per chip from 1970 to 2015, following Moore's Law. For more recent development, in 2020 Apple launched a new chip, called A14 Bionic, processed by a 5 nm node technology, and containing 11.8 billion transistors, which can perform up to 11 trillion operations per second [2].

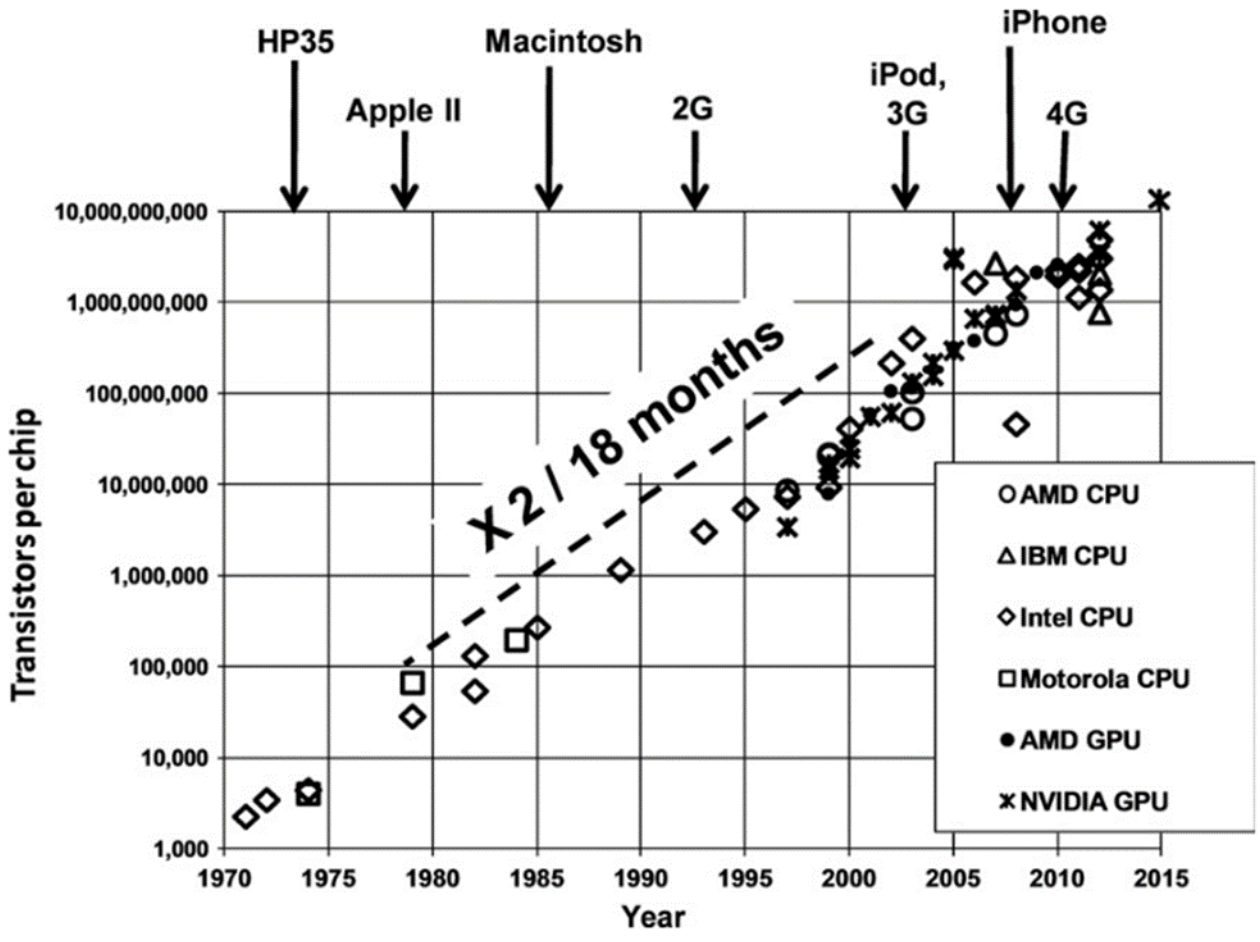

Figure 1 – Evolution of the number of transistors per chip from 1970 to 2015 [1].

In order to support the elevated number of transistors and keep the remarkable performance improvement of the electronic devices, transistors were drastically reduced in size, which implied an interconnect size reduction as well, down to the nanometre scale.

1.1 Copper interconnects

The interconnects are the electronic pathways between transistors in an integrated circuit (IC) and carry electric current. They are separated from the silicon (Si) substrate by a dielectric material, usually silicon dioxide (SiO_2), which works as an insulating layer [3].

Since the late 90's, copper (Cu) has been used as interconnect material in substitution of aluminium (Al), mainly due to its higher conductivity and electromigration resistance. Despite its better electronic properties, copper easily diffuses into Si forming a highly resistive compound (Cu_3Si), which decreases device performance and shortens its lifespan. To avoid this problem, a diffusion barrier layer is required between SiO_2 and Cu [3, 4].

The standard fabrication process for copper interconnects is called Damascene and is represented in Figure 2. The most used is dual damascene process which consists in fabricating both the vias and the lines before filling them with Cu. The vias and the lines are fabricated through SiO_2 patterning and etching. After that, the barrier layer is deposited by physical vapour deposition (PVD), followed by deposition of the Cu-seed layer, also by PVD. Finally, the vias/lines are filled with electrodeposited Cu. The excess copper is then removed by chemical-mechanical polishing [3, 5, 6].

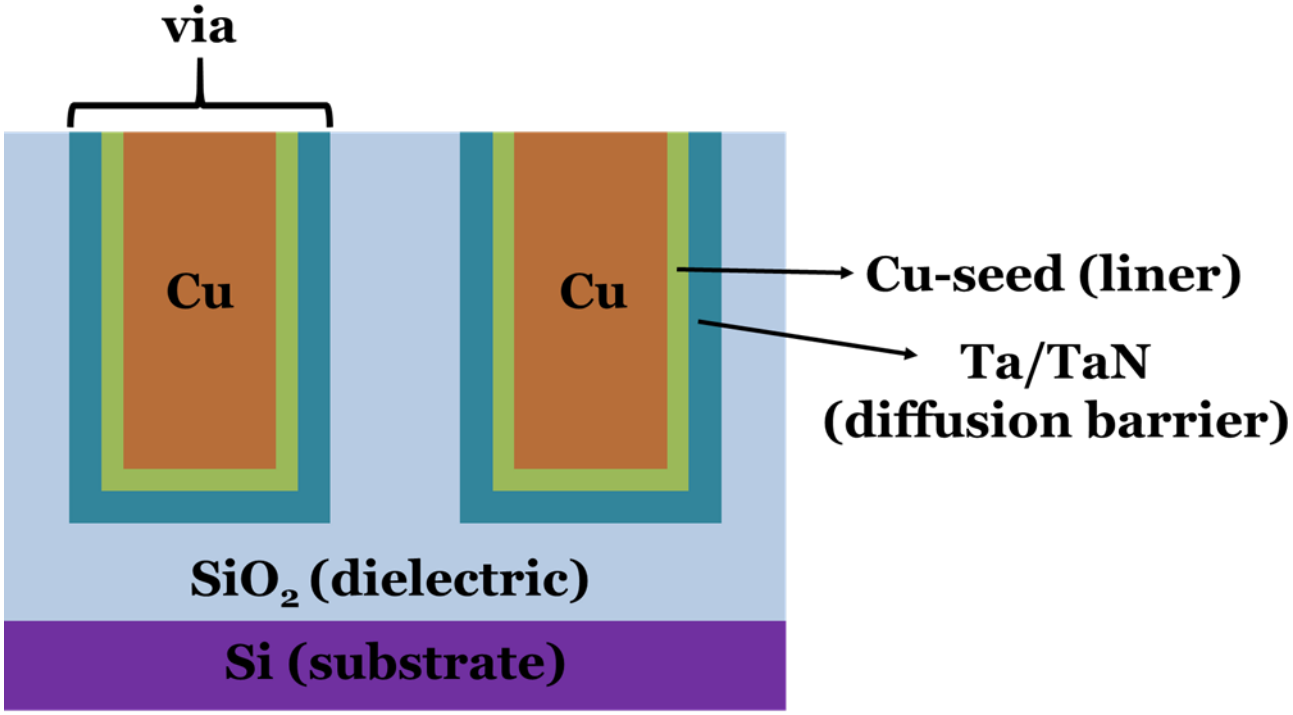

Figure 2 – Schematic representation of the damascene architecture.

1.2 Copper diffusion barriers

The properties of a good diffusion barrier include low copper diffusion coefficient, low resistivity, high thermal stability, good adhesion to SiO_2 and Cu, and chemical inertness

with Cu and Si. Since the diffusion takes place mainly along grain boundaries, amorphous materials are desirable as diffusion barrier layers.

The diffusion barrier must be as thin as possible while granting diffusion barrier properties, since part of the width (W) and height (H) of the interconnect line is constituted by the barrier layer, which affects the interconnect resistance (R), according to equation 1,

$$R = \frac{\rho L}{HW} \quad (1)$$

where ρ is the resistivity and L is the length of the line [4, 5, 7].

1.3 Ta/TaN diffusion barrier

The industry standard for copper diffusion barrier is a bilayer composed by tantalum (Ta) and tantalum nitride (TaN) and it is deposited through PVD. This combination is due to Ta great adhesion properties to Cu and TaN lower Cu diffusion coefficient for grain boundary diffusion ($D'_{0,Cu/TaN} = 2.36 \times 10^{-11} cm^2 s^{-1}$), leading to better diffusion barrier properties than Ta alone ($D'_{0,Cu/Ta} = 9.0 \times 10^{-4} cm^2 s^{-1}$) [3, 5, 8].

Despite the good adhesion properties between Ta and Cu, Ta surface is characterized by the presence of a passivation oxide film, Ta_2O_5, which has poor wettability and adhesion to electrodeposited metals. To solve this problem, a thin Cu-seed layer (liner) is deposited by PVD, previous to via/line filling with Cu by electrodeposition [8, 9].

1.4 Challenges to overcome

Despite the good performance of the Cu/Cu-seed/Ta/TaN/SiO_2/Si stack, its miniaturization leads to two main problems.

Since the Ta/TaN diffusion barrier is more resistive than Cu, the Cu/diffusion barrier volume ratio is decreasing fast as the interconnect dimensions keep shrinking. This means that decreasing the Cu layer width and thickness without any change on the barrier layer thickness, will increase the interconnect resistivity. Alternatively, decreasing Ta/TaN thickness while maintaining the deposition method, PVD, results in a discontinuous and non-uniform film, leading to effectiveness loss as barrier, and ultimately increasing resistivity. In addition, depositing ever-thinning uniform PVD layers is also becoming a process challenge for both the diffusion barrier and the Cu-seed [10].

Figure 3 shows the increase in the effective resistivity for Cu/Ta/TaN stack as a function of the decrease in technology node. The 10, 7, 5 and 3 nm lines represent different barrier layer thicknesses, and the dashed grey line represents the desired diffusion barrier layer thickness to maintain the resistivity at 2.2 mΩ.cm, which is the recommended value by the International Technology Roadmap for Semiconductors (ITRS), for each technology node. Accordingly, as the technology node progresses, either thinner diffusion barrier layers are required or the resistivity will increase [10, 11].

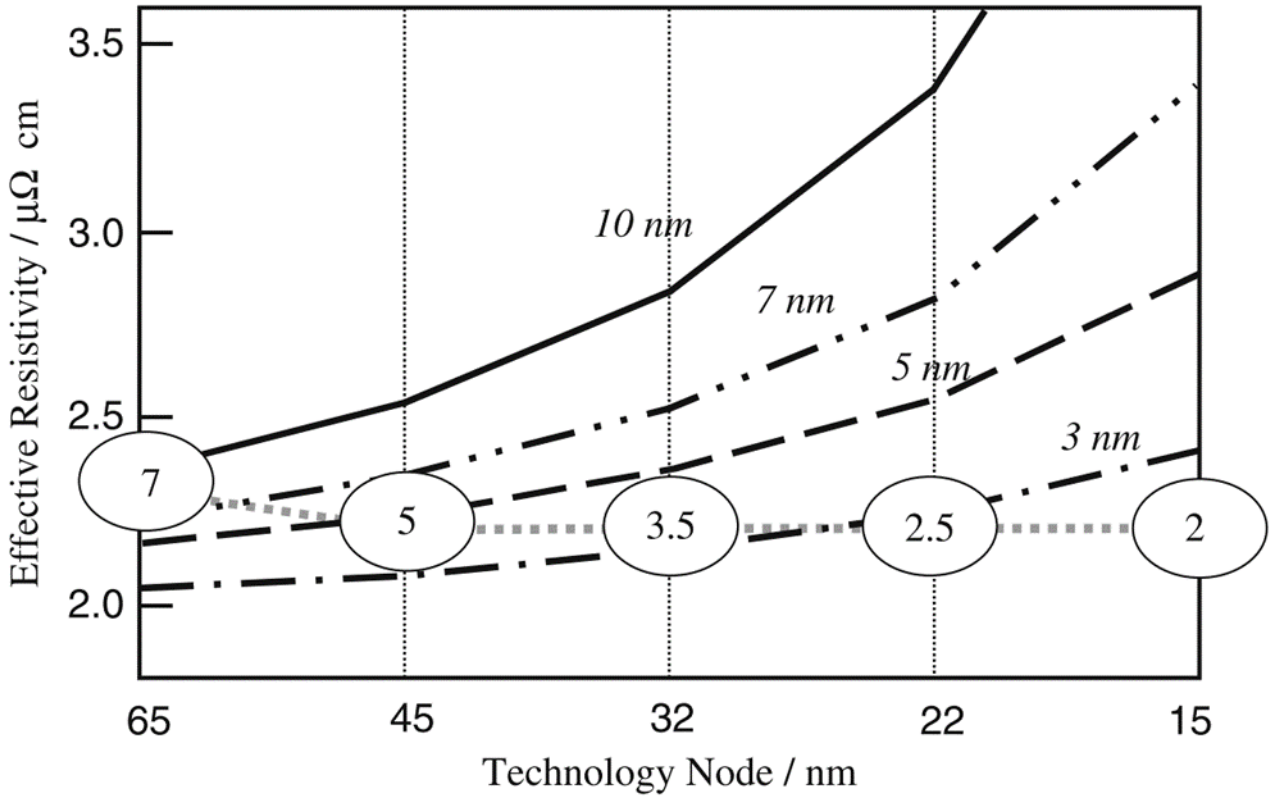

Figure 3 - Effective resistivity for Cu/Ta/TaN stack as function of the technology node [10].

To address these problems in an effort to uphold the Cu interconnect paradigm, alternative materials have been considered to act as Cu diffusion barriers, which should desirably allow direct Cu electroplating, avoiding the need of a Cu-seed layer. Alternative deposition methods, such as chemical vapour deposition (CVD) and atomic layer deposition (ALD), or improvements of PVD conditions to obtain thin and continuous films are also being studied to allow the interconnects miniaturization while also maintaining the recommended resistivity.

2. Literature Review

Tungsten-based diffusion barriers are promising candidates to replace Ta/TaN layers, due to their high melting point and thermal stability. On top of that, W is being used in the semiconductor industry as contact material between transistors and interconnects for microprocessor fabrication. However, W microstructure has a strong tendency to columnar grain growth, which acts as diffusion paths for Cu atoms. Therefore, it must be coupled with other materials to enhance diffusion barrier properties [5].

This chapter focuses on two W-based systems, namely Co-W and Ru-W.

2.1 Co-W diffusion barriers

Cobalt can form a highly adhesive interface with Cu, has high electrical conductivity and high melting temperature. However, pure Co has poor Cu diffusion barrier properties and is easily dissolved in low pH solution, which makes direct (seedless) Cu electroplating a challenging task. When coupled with W, Co presents good adhesion to copper and lower resistivity than TaN, as well as improved diffusion barrier properties [5].

The study of the Co-W system, regarding its diffusion barrier properties, direct Cu plating capability, Cu wetting ability, as well as the influence of W in Co dissolution is scarce in the literature [12-14]. These studies include different deposition methods for Co-W film deposition, such as ALD, CVD and PVD.

2.1.1 Diffusion barrier properties

Su *et al*. [12] studied the effect of W incorporation in Co-W alloys, to act as seedless diffusion barriers. The Co-W films were prepared by PVD with different W/Co atomic ratio, which was achieved by changing the W radio frequency (RF) sputtering power (20 to 60 W). Figure 4 demonstrates the correlation between W RF power and the W/Co atomic ratio.

To study adhesion and diffusion barrier properties, a 50 nm-thick Cu film was deposited by PVD, forming Cu/Co-W/Si stack. The authors also studied Cu/Si and Cu/TaN/Si stacks, for comparison. The samples were submitted to rapid thermal annealing (RTA) at 400 °C, for 30 min, to observe adhesion properties as well as Cu silicide formation.

The diffusion properties of Co-W films were analysed through *in situ* sheet resistance measurements, according to Figure 5, in a furnace with a ramp rate of 10 °C/min.

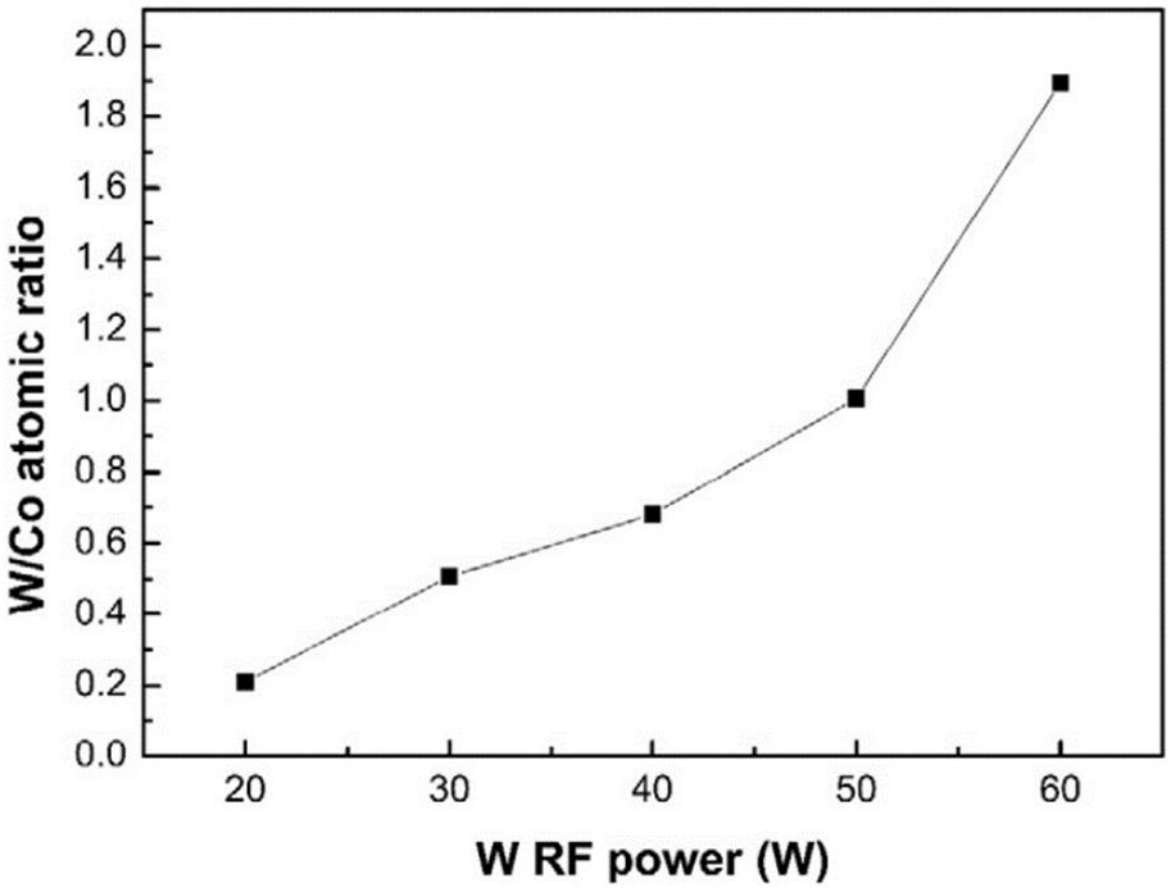

Figure 4 - W/Co atomic ratio with the variation of W RF power [12].

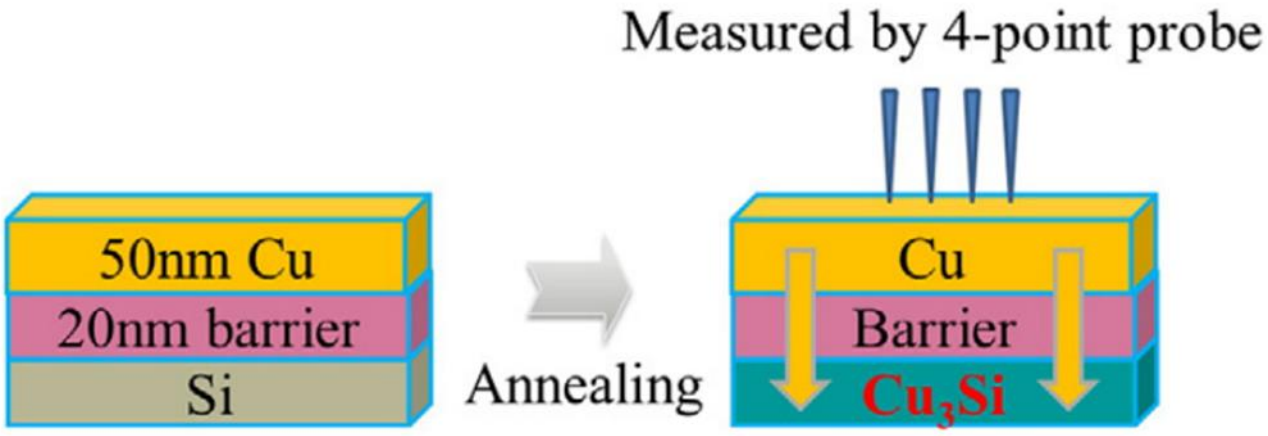

Figure 5 – Schematic representation of the in situ sheet resistance measurements [12].

Figure 6 shows the *in situ* sheet resistance measurements for Cu/Si, Cu/TaN/Si and Cu/Co-W/Si, with different W/Co atomic ratio, as function of the annealing temperature. For the sample with no diffusion barrier, Cu/Si, an abrupt increase of the sheet resistance is observed when the sample hits 400 °C. This indicates the formation of Cu silicide due to Cu diffusion into silicon. For Cu/TaN/Si stack, the increase in the sheet resistance

appears only at 650 °C, meaning barrier failure at this temperature. For Co-W diffusion barriers, the barrier failure temperature increases with the increasing of the W/Co atomic ratio. The sample with W/Co atomic ratio of 1.9 shows the same performance as TaN diffusion barrier.

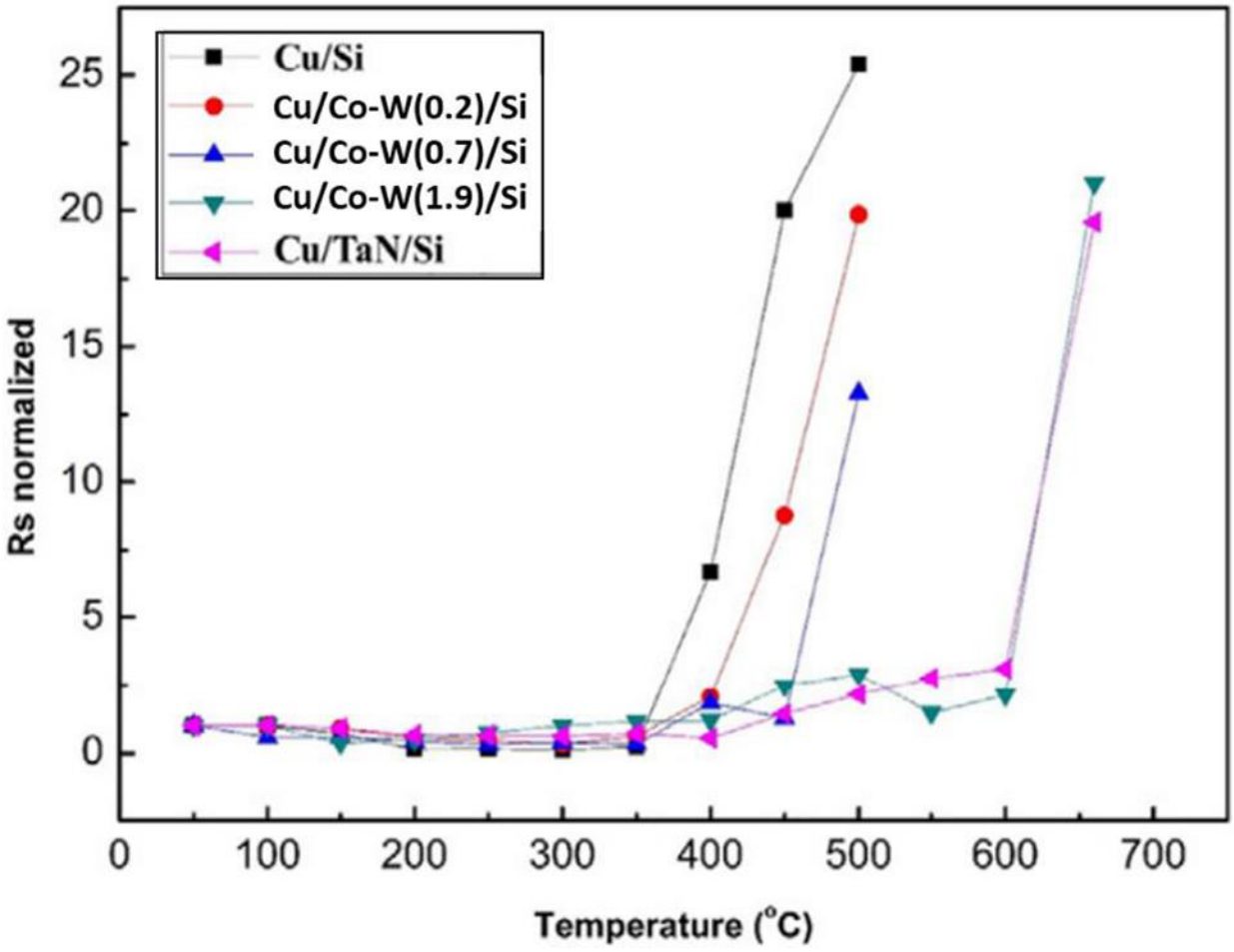

Figure 6 - Normalized sheet resistance of Cu/Si, Cu/Co-W(0.2)/Si, Cu/Co-W(0.7)/Si, Cu/Co-W(1.9)/Si and Cu/TaN/Si stack in function of annealing temperature. Adapted from [12].

Shimizu *et al.* [13] studied the diffusion barrier properties of Co-W films as cap layers, which are deposited on top of the Cu interconnects, preventing Cu diffusion to the upper SiO_2 insulating layer. The films were deposited by CVD, with two concentrations of W (10 and 20 % at.) and three different thicknesses (10, 20 and 30 nm) on EP-Cu/PVD-TaN/Si stack (Figure 7). The samples were annealed at 400, 500 and 600 °C for 5 minutes followed by resistivity measurements and X-ray photoelectron spectroscopy (XPS) analysis. For comparison, the authors also studied Co/EP-Cu/PVD-TaN/Si samples, under the same conditions.

Figure 8 shows the surface coverage of copper for Co and Co-W diffusion barriers, for different thicknesses at different annealing temperatures. The surface coverage is the amount of Cu, in nm, that diffuses through the barrier, meaning that the higher the surface coverage, the higher the amount of Cu atoms that diffuse to the surface. As

expected, the surface coverage of copper increases with the increase of the annealing temperature and decreases with the increase of the film's thickness and W content.

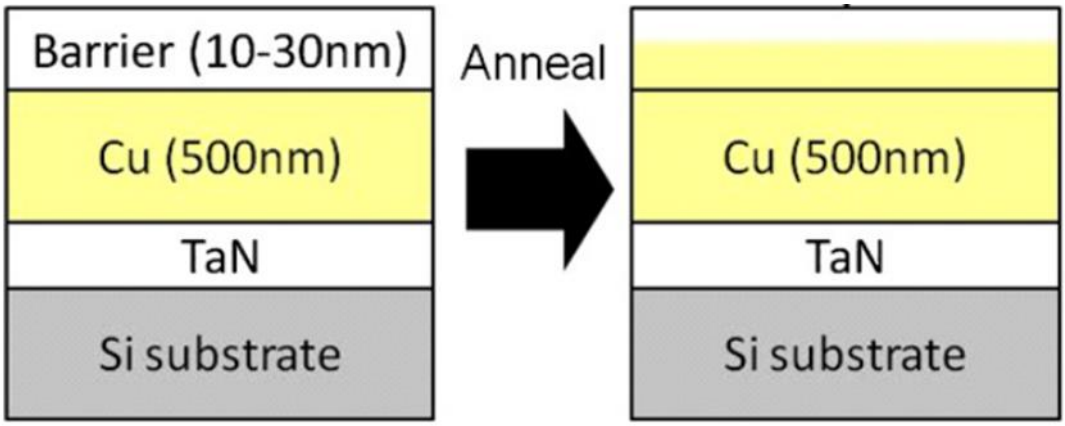

Figure 7 – Evaluation method for barrier properties against Cu diffusion [13].

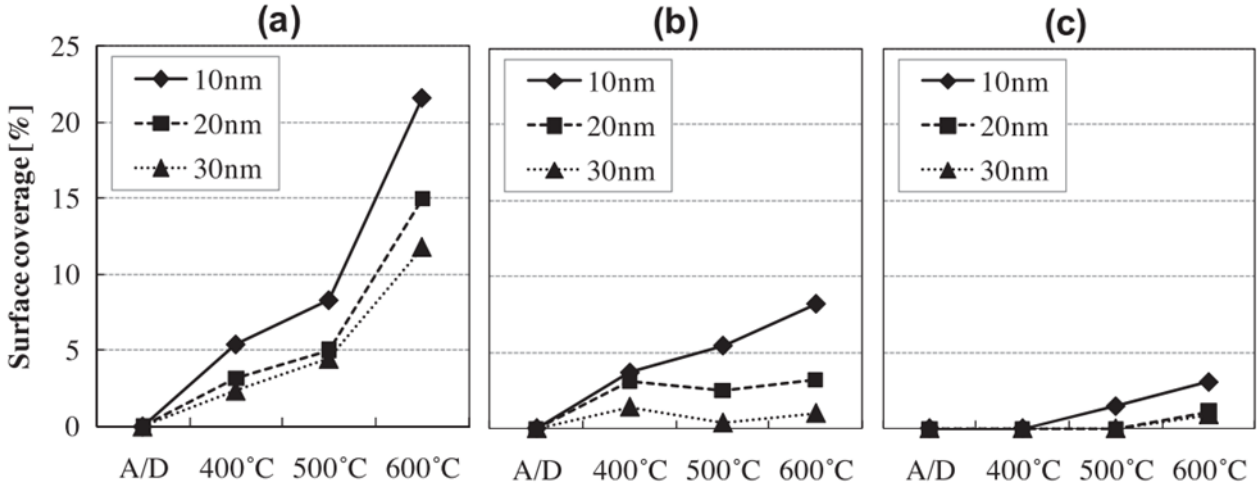

Figure 8 – Surface coverage of Cu for a) CVD-Co, b) CVD-Co-W(10) and c) CVD-Co-W(20) for as-deposited condition and annealed at different temperatures [13].

In order to explain the better performance of Co-W as Cu diffusion barrier, the authors proposed 3 hypotheses. First, they observed the formation of an intermetallic compound between Co and W, Co_3W, as shown in Figure 9, that could be "stuffed" at Co grain boundaries, preventing Cu from diffusing. Second, Cu and Co_3W do not form a solid solution, which prevents Cu diffusion in Co_3W grains. In the third hypothesis, the authors observed the formation of a nanostructure of amorphous Co by adding W to explain the improved diffusion barrier performance of higher W content layers.

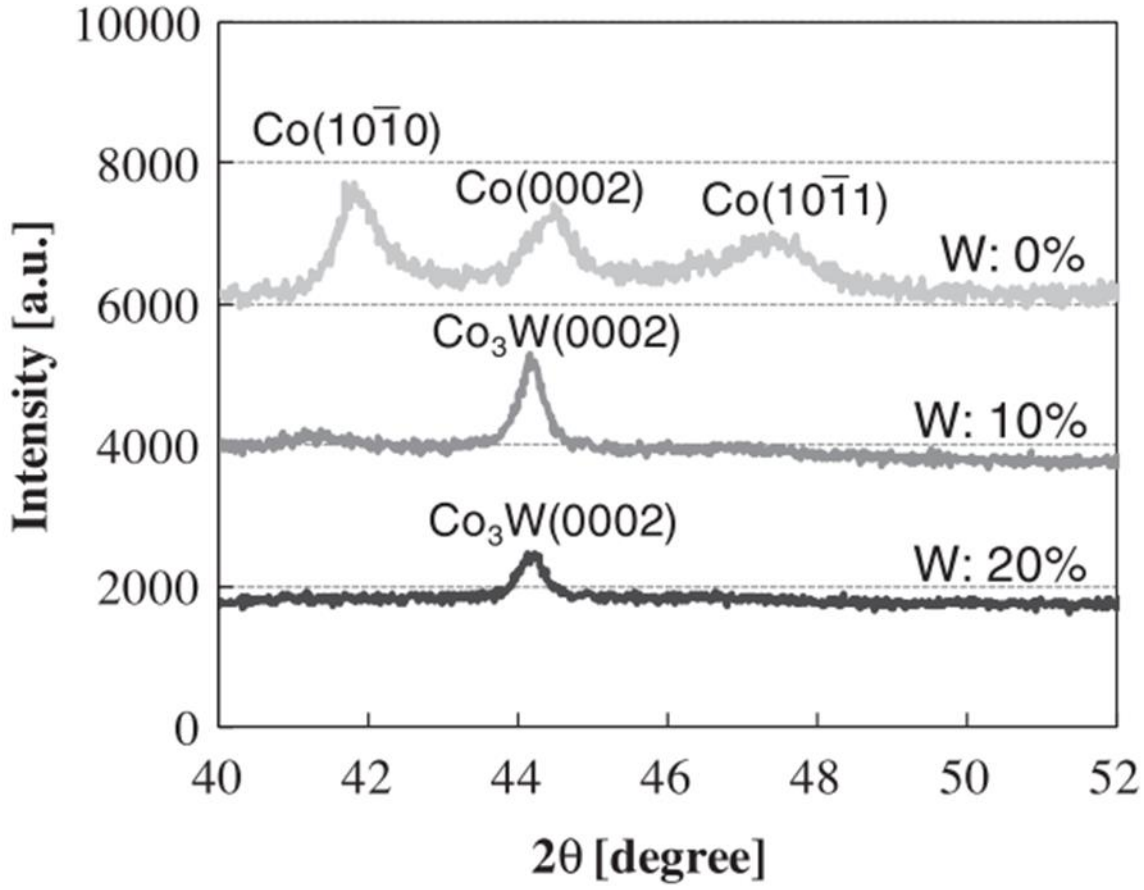

Figure 9 – X-ray diffraction (XRD) analysis of CVD-Co and CVD-Co-W films [13].

In a different work [14], the same authors studied Co-W diffusion barriers deposited by ALD. They prepared oxygen-free Co-W films with different concentration of W, by altering gas-feed sequence in ALD process.

To evaluate the diffusion barrier properties, 20 nm-thick Co-W and Co films, for comparison, were deposited on a Cu substrate, to form a diffusion couple (Cu/Co and Cu/Co-W). The samples were annealed at 400, 500 and 600 °C, for 5 to 750 min in 50 Torr of H_2 atmosphere. The depth profile of Cu concentration (C(z)), which indicates the amount of Cu that diffuses into the substrate as well as how deep Cu atoms penetrate, was measured by XPS and calculated by equation 2,

$$C(z) = \frac{100}{\sqrt{2\pi\sqrt{Dt}}} \int_0^z \exp\left[-\left(\frac{\zeta - z_0}{2\sqrt{Dt}}\right)^2\right] d\zeta \qquad (2)$$

where D is the diffusion coefficient, t is the annealing time and z_0 is the position of 50 % of concentration.

Figure 10 shows the diffusion depth profiles of Cu/Co and Cu/Co-W films. For Cu/Co (Figure 10a), the profile changed drastically after annealing at 500 and 600 °C, indicating Cu diffusion into Co. This behaviour is not observed for Cu/Co-W films, where the profile remains almost the same after annealing, as can be seen in Figure 10b.

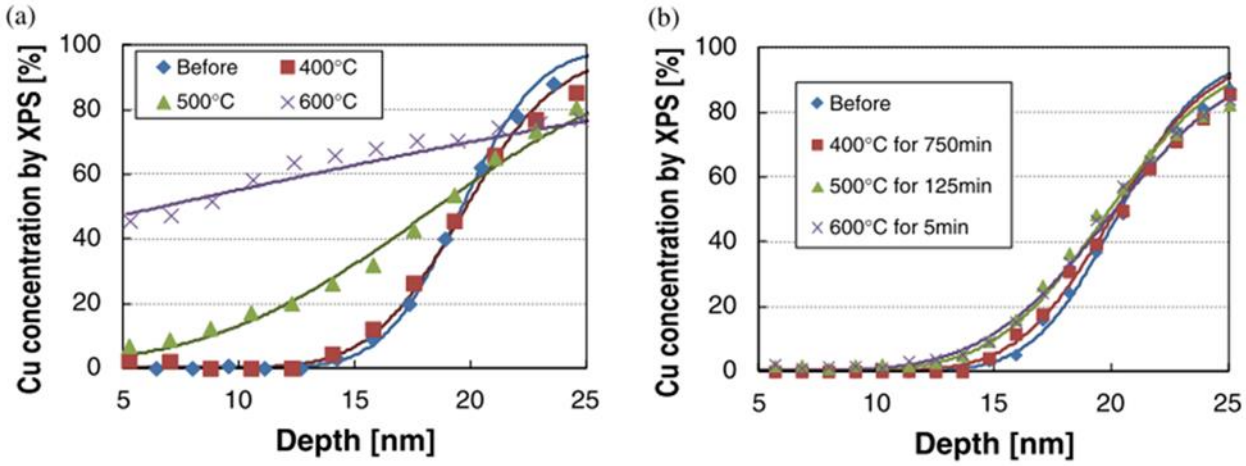

Figure 10 – Diffusion profiles of a) Cu/Co and b) Cu/Co-W films [14].

Cu diffusion coefficient on ALD-Co and ALD-Co-W, calculated from equation 2, can be seen in Figure 11. The dashed line represents the lowest Cu diffusion coefficient previously reported on TaN. As observed, Cu diffusion coefficient on Co-W films (10% of W) is lower than on Co, which means that Co-W has better diffusion properties. The authors also reported that the Cu diffusion coefficient on Co-W films with 10 % of W, bellow 400 °C, was as low as on TaN at the same temperature.

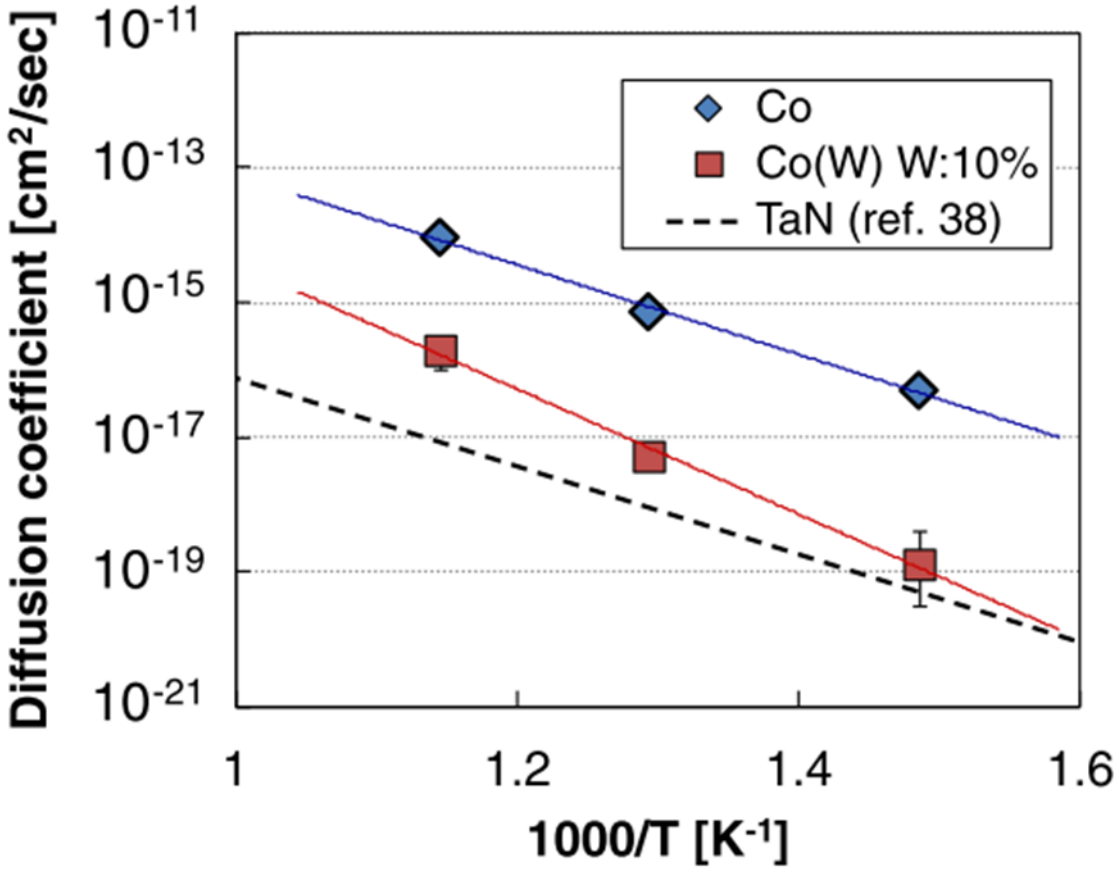

Figure 11 - Cu diffusion coeficient on ALD-Co and ALD-Co-W films [14].

This effect was attributed to the presence of an amorphous phase on the Co grain boundaries, that is formed with addition of W, which can be observed by the XRD diffractogram in Figure 12. With the addition of W, the intensity of the Co peak (44.3 °) decreases, indicating the formation of an amorphous phase.

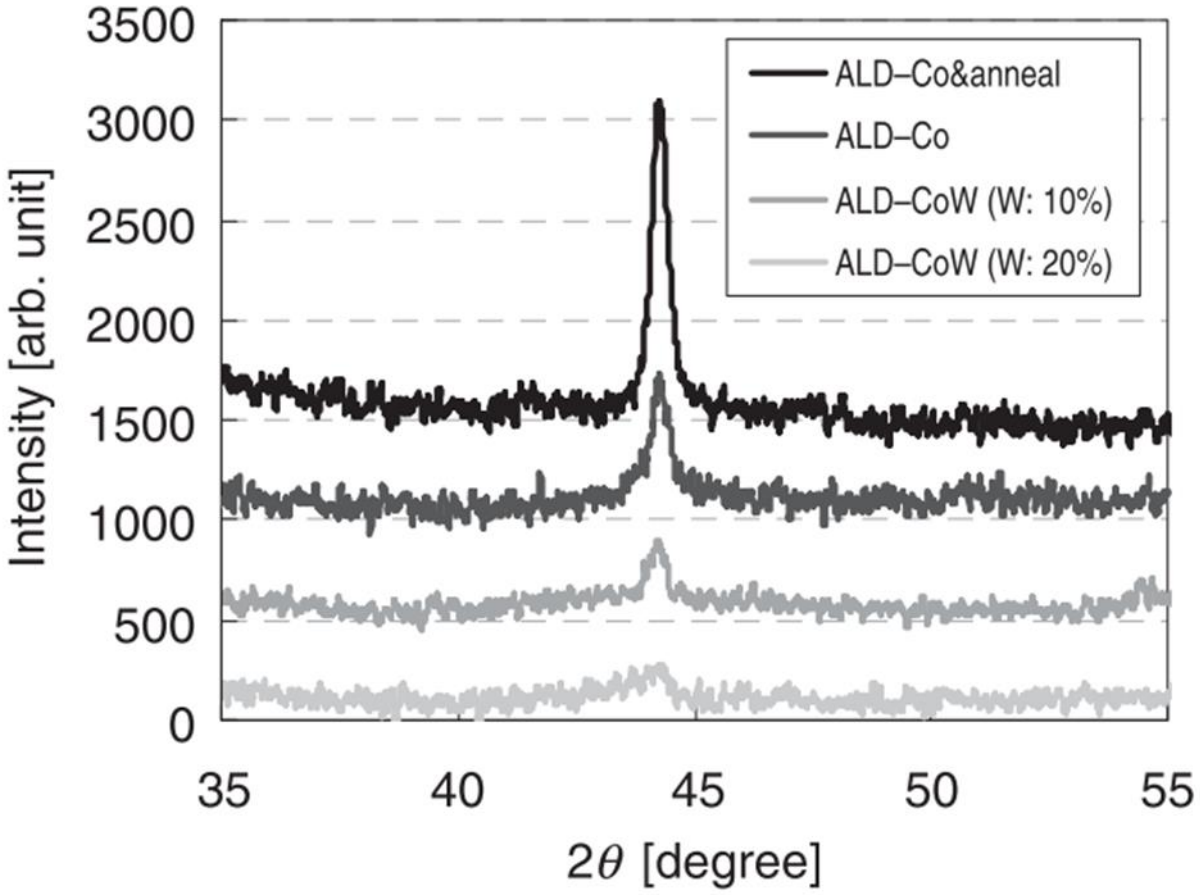

Figure 12 – XRD diffractogram of Co and Co-W films [14].

2.1.2 Direct copper plating and wetting ability

The direct copper plating capability and the wetting ability can be evaluated by the morphology and thermal stability of Cu films deposited on Co-W.

Su *et al*. [12] studied the direct Cu electrodeposition for 1, 5, 15 and 60 seconds, on different substrates. The electrolyte was an acidic solution containing 0.05 M $CuSO_4$, 0.05 M H_2SO_4. The samples were observed by scanning electron microscopy (SEM), and the results can be seen in Figure 13. The authors identified 3 different situations. First, when Cu was electroplated on Ta, TaN or W, a progressive nucleation can be observed as well as a deposit formation with a large difference in size, which will lead to a rough and discontinuous film. Second, when Cu was electroplated on Co, there was almost no film formation, due to Co dissolution caused by the electrolyte solution. And third, when Cu was electroplated on Co-W, an instant nucleation and homogeneous growth can be observed, making it possible to electroplate a continuous and smooth Cu film on Co-W substrate. However, despite this statement, the authors did not present an image of a continuous and homogeneous Cu electroplated film on Co-W.

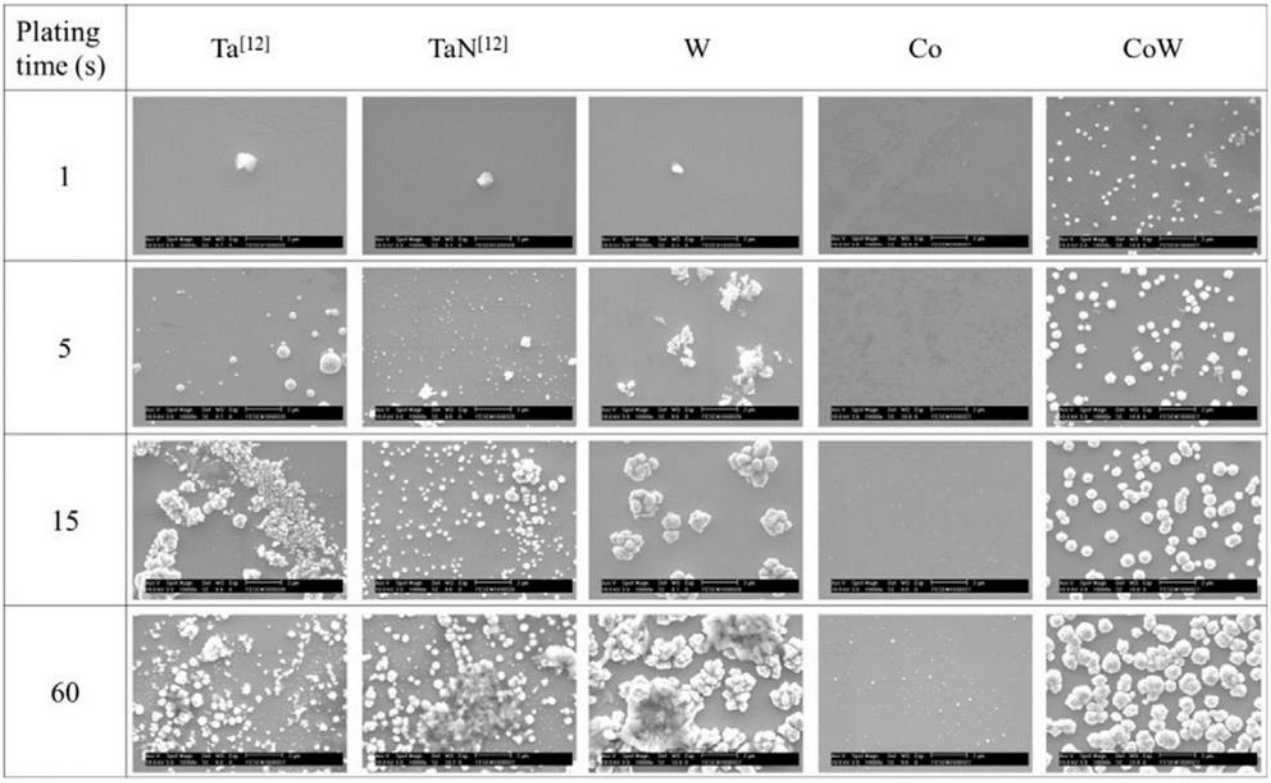

Figure 13 - SEM images of different barrier films after Cu electroplating for 1, 5, 15 and 60 seconds [12].

The authors also studied Cu electrodeposition on Co-W substrates with different W/Co atomic ratio (Figure 14). As can be observed, almost no Cu was electroplated on Co-W(0.2) and Co-W(0.5) substrate as Co dissolution can still be seen in this two substrates. For Co-W(0.7) small clusters are present, which was characterized by energy dispersive X-ray spectroscopy (EDS) as mainly W atoms and a few Co-W alloys, indicating that at this W concentration still occurs Co dissolution. For Co-W(1.0) and Co-W(1.9) it is observed high density of Cu nuclei and uniform growth.

Table 1 shows Cu nuclei density and nuclei size for Co-W(1.0) and Co-W(1.9). As can be seen, Cu nuclei density and size for the Co-W(1.0) is slightly higher than for the Co-W(1.9). Also, as seen in Figure 13, Cu nuclei density on pure W films is very low. This indicates that although Cu films can be electroplated on Co-W, the increase in the W content could lead to a low Cu nuclei density.

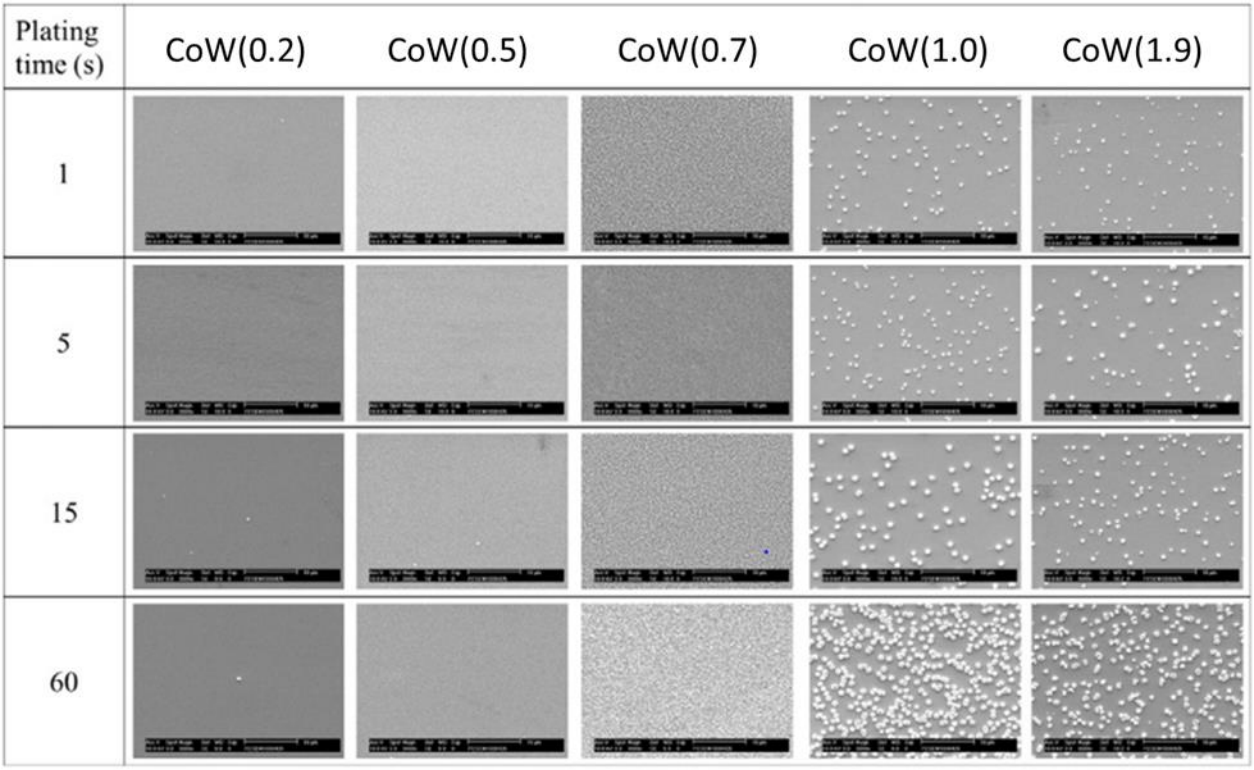

Figure 14 - SEM images of Co-W films, with different W/Co atomic ratio, after Cu electroplating for 1, 5, 15 and 60 seconds [12].

Table 1 - Nuclei density and nuclei size of electroplated Cu on Co-W(1.0) and Co-W (1.9) [12]

Substrate	Nuclei density (cm^{-2})	Nuclei size (μm)
Co-W(1.0)	1.6×10^{10}	0.95
Co-W(1.9)	9.1×10^{9}	0.90

As mentioned before, pure Co films tend to dissolve in low pH solutions, such is the case in standard baths for Cu electroplating. Therefore, under these conditions Cu cannot be electroplated on top of pure Co, as seen in Figure 13.

To study Co dissolution, the authors [12] performed a dipping test, where Co-W(0.2) and Co-W(1.0) films were dipped in the same solution used as electrolyte for Cu deposition, for 1 second. After that, the samples were observed by transmission electron microscopy (TEM).

Figure 15 shows cross-section TEM images of the samples as-deposited and after dipping. As can be observed, Co-W(0.2) thickness decreased by more than half after dipping in the acidic bath. Meanwhile, Co-W(1.0) thickness remained almost the same, with a slight change in the film roughness. As seen before, only at higher concentrations of W, Co dissolution will be suppressed. The authors explain that the small amounts of W will not be enough to form alloy with Co, and its structure will remain mostly crystalline,

as columnar grains can be seen in Figure 15a. In the meantime, Figure 15c shows an amorphous-like structure which is less susceptible to corrosion.

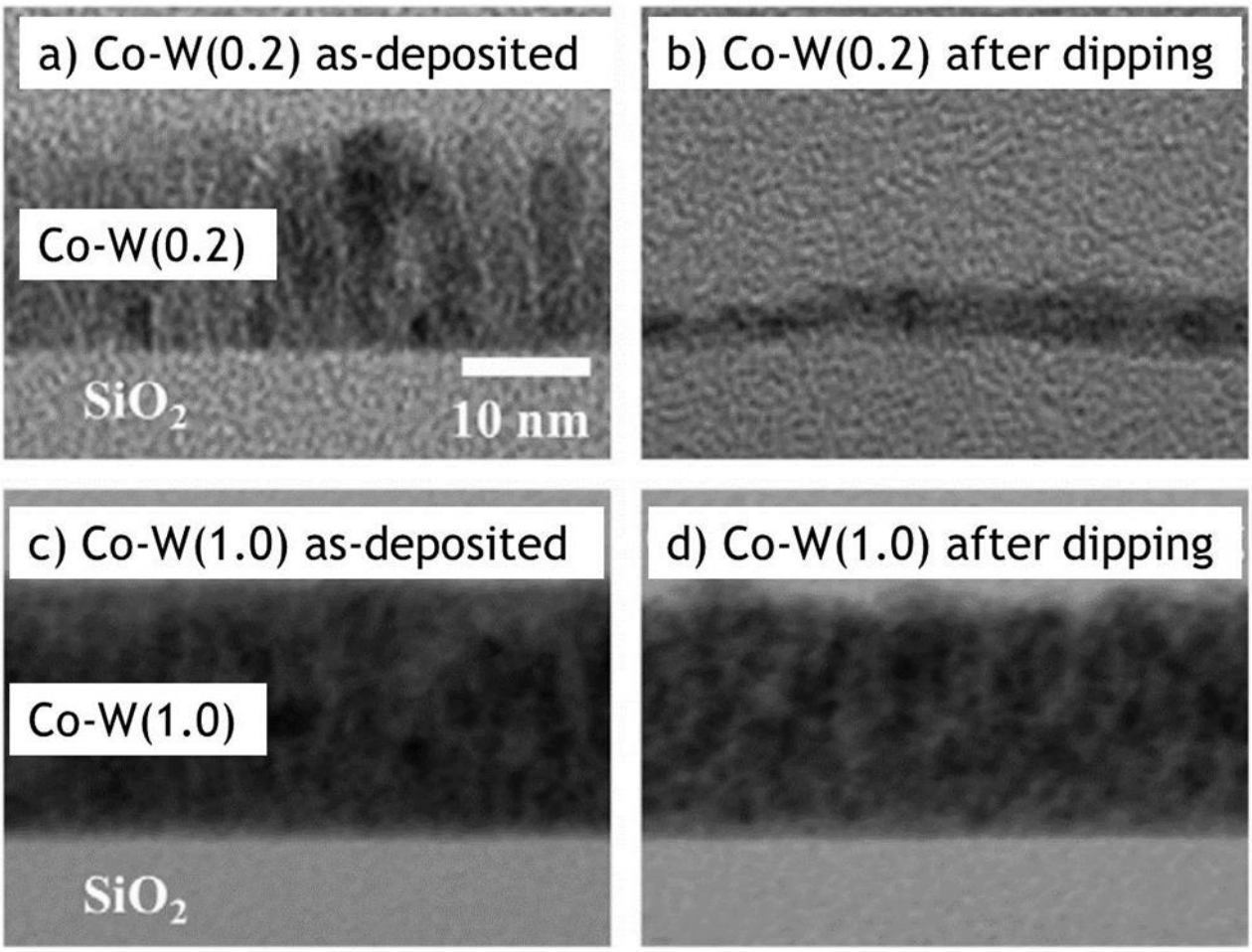

Figure 15 - TEM images of a) Co-W(0.2) as-deposited, b) Co-W(0.2) after dipping, c) Co-W(1.0) as-deposited and d) Co-W(1.0) after dipping. Adapted from [12].

A study on the direct copper plating capability of Co-W thin films was previously developed by Santos, R. F. *et al.* [15], that investigated the early stages of formation of Cu film electroplated on Co-W substrate, in low pH electrolyte. Co-W thin films with equimolar composition were deposited by direct-current (DC) magnetron sputtering and Cu electroplating was carried out in an acidic Cu sulphate solution (pH < 2).

The authors investigated the effect of both DC and pulsed-current (PC) on Cu electrodeposition on Co-W. However, even with different current densities and deposition times, the authors were not able to obtain a continuous and uniform Cu film (Figure 16). This was attributed to Co preferential dissolution in the electrolyte, which was reported before [12].

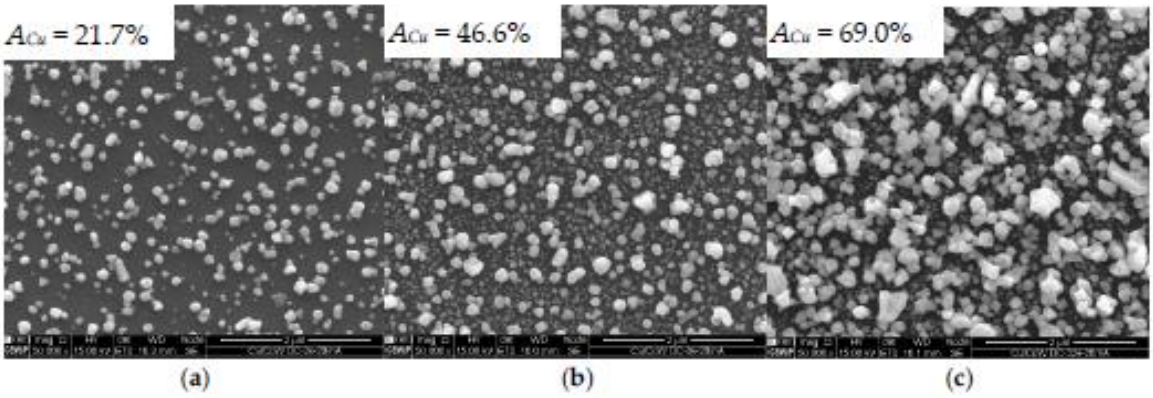

Figure 16 – Cu electrodeposited on Co-W by DC at (a) 20 mA·cm^{-2}, for (a) 2, (b) 8 and (c) 32 s [15].

In an attempt to overcome this issue, the authors prepared a less aggressive version of the electrolyte, by adding drops of concentrated NaOH to the original electrolyte, until pH 3.5 was reached. This modified electrolyte was used to electroplate Cu films on Co-W with DC density of 10 mA·cm^{-2} (Figure 17a). The cross-sectional image (Figure 17b) reveals a dense and continuous Cu film, indicating that the higher pH electrolyte (pH = 3.5) is less damaging to Co-W substrate.

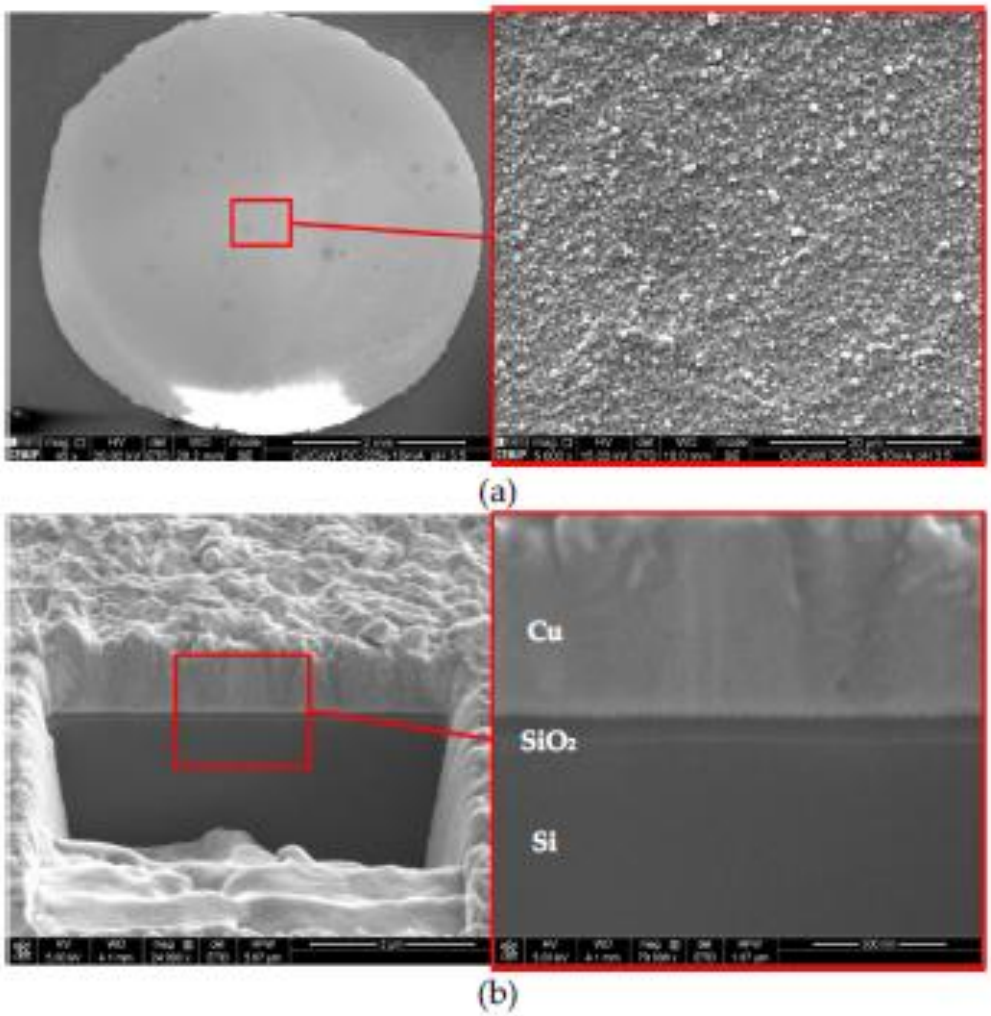

Figure 17 - (a) Film surface and (b) cross-section of Cu film electroplated on Co-W by DC at 10 mA·cm−2 for 225s, in modified electrolyte (pH 3.5) [15].

To evaluate the wetting ability of Cu on Co-W, Su et al. [12] submitted a 50 nm- thick Cu film, deposited by PVD on Co-W/SiO_2, to RTA for 30 min at 400 °C. The samples were characterized by SEM and the results are shown in Figure 18. The authors also deposited Cu on Ta to compare adhesion properties.

After RTA, Cu agglomeration and pinholes formation is observed which can be related to the barrier wetting ability, as larger agglomeration and larger pinholes indicate poor wetting ability. As expected, it is observed that for higher W concentration, the worse the wetting ability. However, the wetting ability of Co-W(1.0) and Co-W(1.9) is comparable to Ta wetting ability.

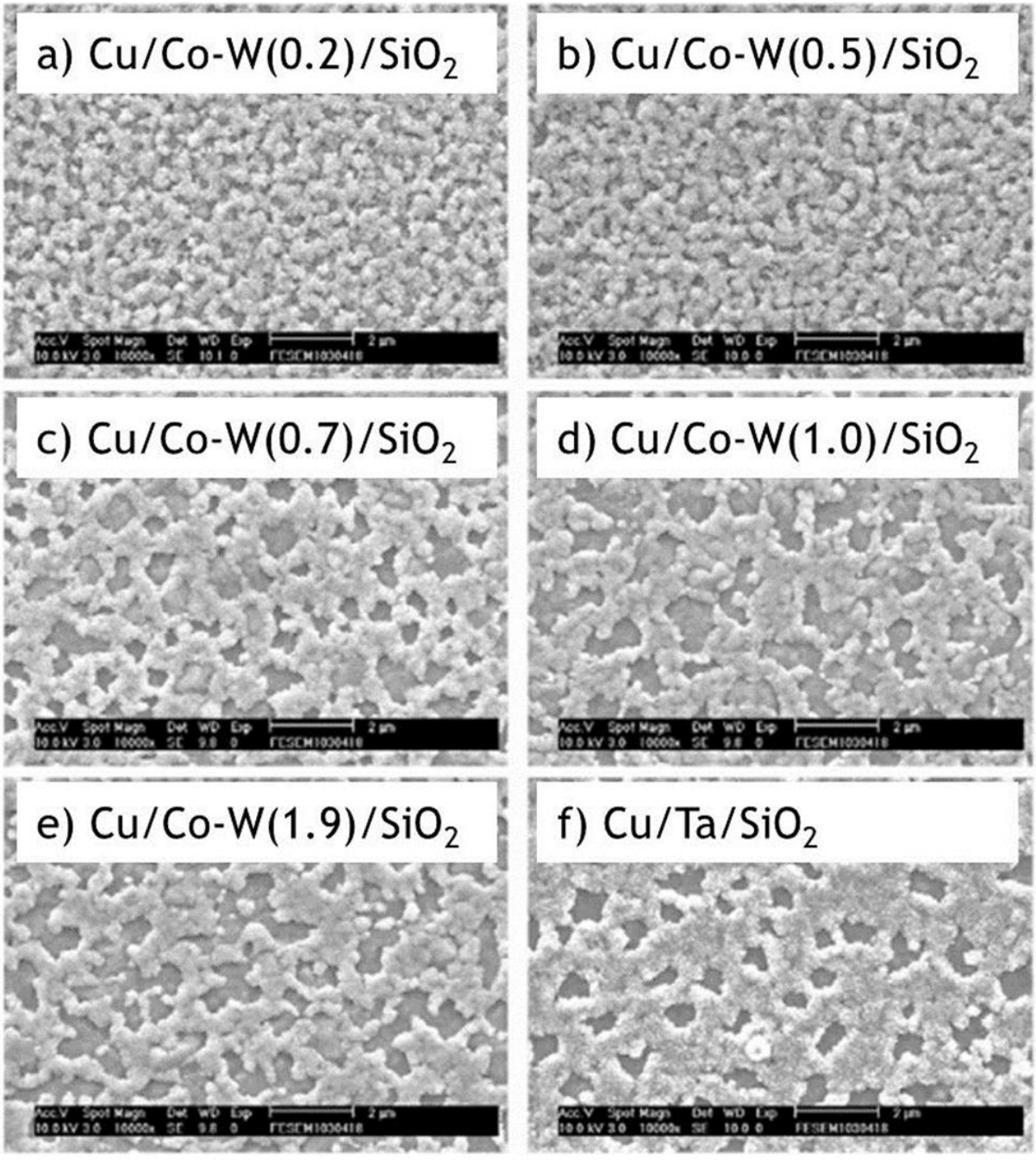

Figure 18 - SEM images of Cu/Co-W(0.2)/SiO_2, Cu/Co-W(0.5)/SiO_2, Cu/Co-W(0.7)/SiO_2, Cu/Co-W(1.0)/SiO_2, Cu/Co-W(1.9)/SiO_2 and Cu/Ta/SiO_2 stacks after RTA. Adapted from [12].

2.2 Ru-W diffusion barriers

Ruthenium is a hard metal with good thermal stability and high electrical conductivity. The absence of intermetallic compounds between Ru and Cu, as well as the good adhesion properties between them, make Ru a promising candidate to replace Ta/TaN diffusion barriers. However, it needs to be coupled with other materials, such as W, to enhance the diffusion barrier properties [16].

Very few results have been reported in the literature on the Ru-W system alone, regarding its copper diffusion barrier properties, the direct copper plating and wetting ability. A few studies focused on the effect of the addition of other materials, such as nitrogen (N) and carbon (C) in some of these properties [17-19].

2.2.1 Diffusion barrier properties

Kuo *et al.* [17] studied the diffusion barrier properties, as well as the plating and wetting ability of Ru-W multi-layers for copper metallization. Ru and W layers were deposited on SiO_2/Si substrate by DC magnetron-sputtering. Different RF sputtering power was applied at the W target, in order to produce films with different W/Ru atomic ratio, as can be seen in Figure 19. Table 2 shows the correlation between the RF power and the W/Ru atomic ratio.

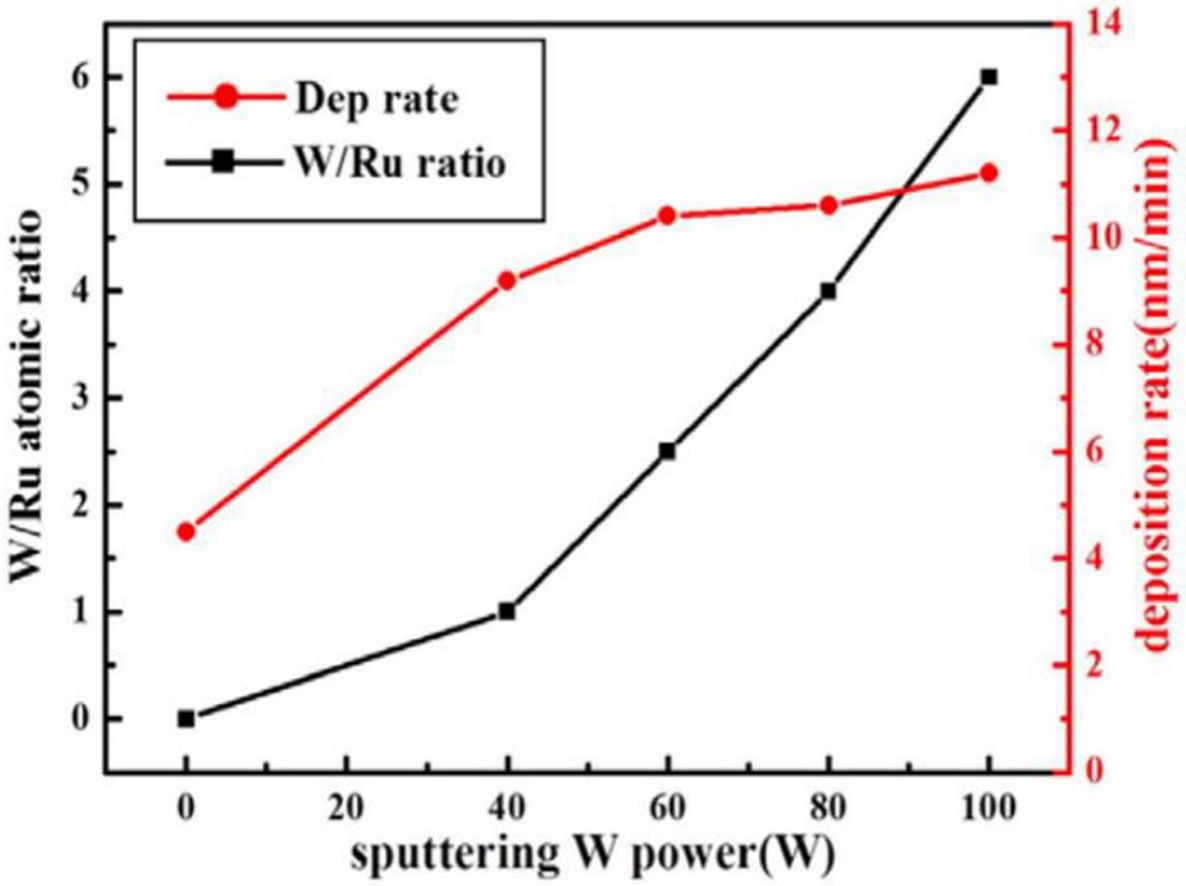

Figure 19 - Atomic ratio of Ru-W films with the variation of the RF sputtering W power [17].

Table 2 – Correlation between the RF power and the W/Ru atomic ratio [17]

RF Power (Watts)	40 W	60 W	80 W	100 W
W/Ru atomic ratio	1	2.5	4	6

To investigate the diffusion barrier properties, Cu/Ru-W/Si stacks were submitted to RTA for 30 min at 500 °C as well as Cu/Ru/Si, Cu/W/Si and Cu/Si stacks, for comparison. The samples were analysed by SEM and XRD. The Cu deposition method was not specified.

Figure 20 shows SEM surface images of the Cu/Ru-W/Si, Cu/Ru/Si, Cu/W/Si and Cu/Si stacks. As can be seen, the images show the presence of bubbles, which the authors attributed to the formation of Cu_3Si, although the source they cite to support such statement does not seem to provide strong evidence to correlate the bubbles appearance to the copper silicide formation. For Figure 20a, with no diffusion barrier between Cu and Si, the formation of Cu_3Si was expected. For Cu/Ru/Si and Cu/W/Si, in Figure 20b and Figure 20g, the bubble formation was elevated, indicating that pure Ru and W are not effective as Cu diffusion barrier after RTA for 30 min at 500 °C. For Ru-W system, the bubbles appear in higher number for Ru-W(1) and Ru-W(6). However, for Ru-W(2.5) and Ru-W(4), almost no bubble is formed, indicating that Cu did not diffuse through those barriers, at 500 °C. The authors attributed this behaviour by the possible formation of an amorphous-like structure between Ru and W, at 2.5 and 4 W/Ru atomic ratios. The study does not provide, however, an explanation on why intermediate W/Ru ratios promote an amorphous-like structure to Ru-W films.

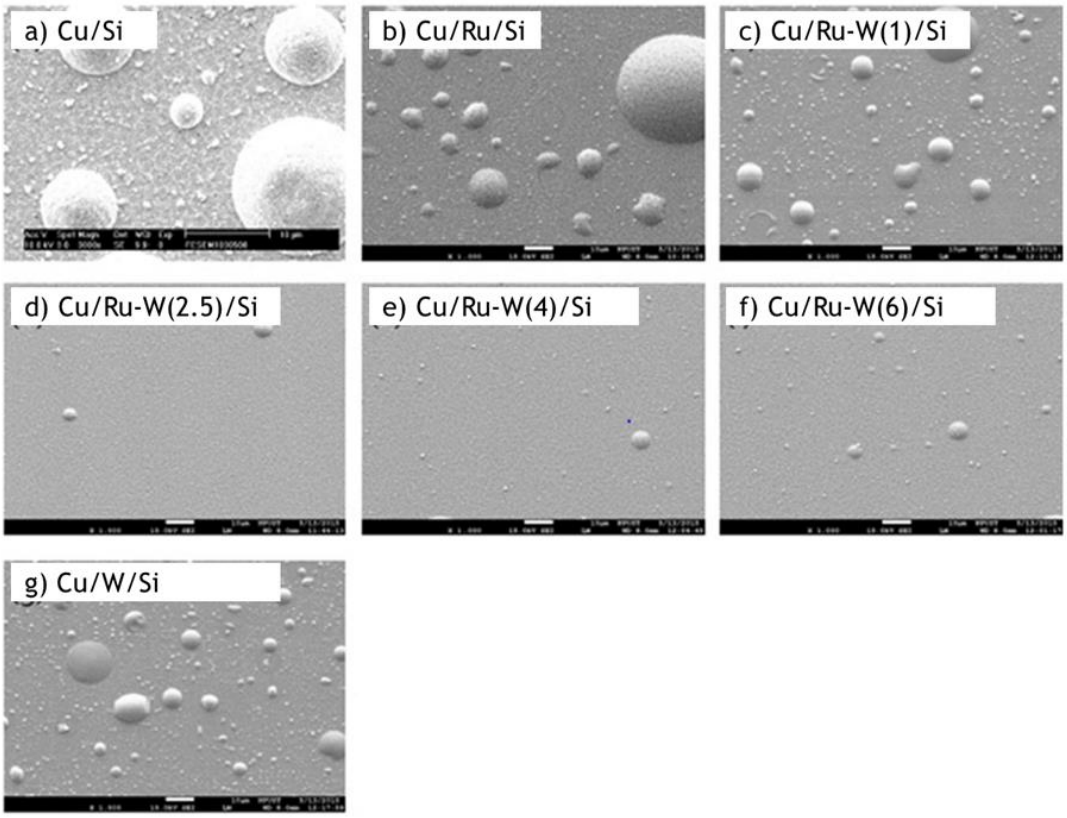

Figure 20 – SEM imagens of Cu electroplated on different substrates, after RTA for 30 min at 500 °C [17].

The XRD patterns for Cu/Ru-W(2.5)/Si stack as-deposited and annealed for 30 min at 500, 600 and 700 °C can be seen in Figure 21. An increase in the two Cu peaks (2θ = 43.3, 50.6) can be observed after annealing at 500 °C, which can be assigned to grain growth. The authors point to the presence of Cu silicide peaks only at 700 °C (2θ = ~44.5, 45), indicating Cu diffusion into Si at this temperature. However, a small peak (2θ = ~44.5) appears at 600 ºC, which could indicate that Cu diffuses into Si before 700 ºC.

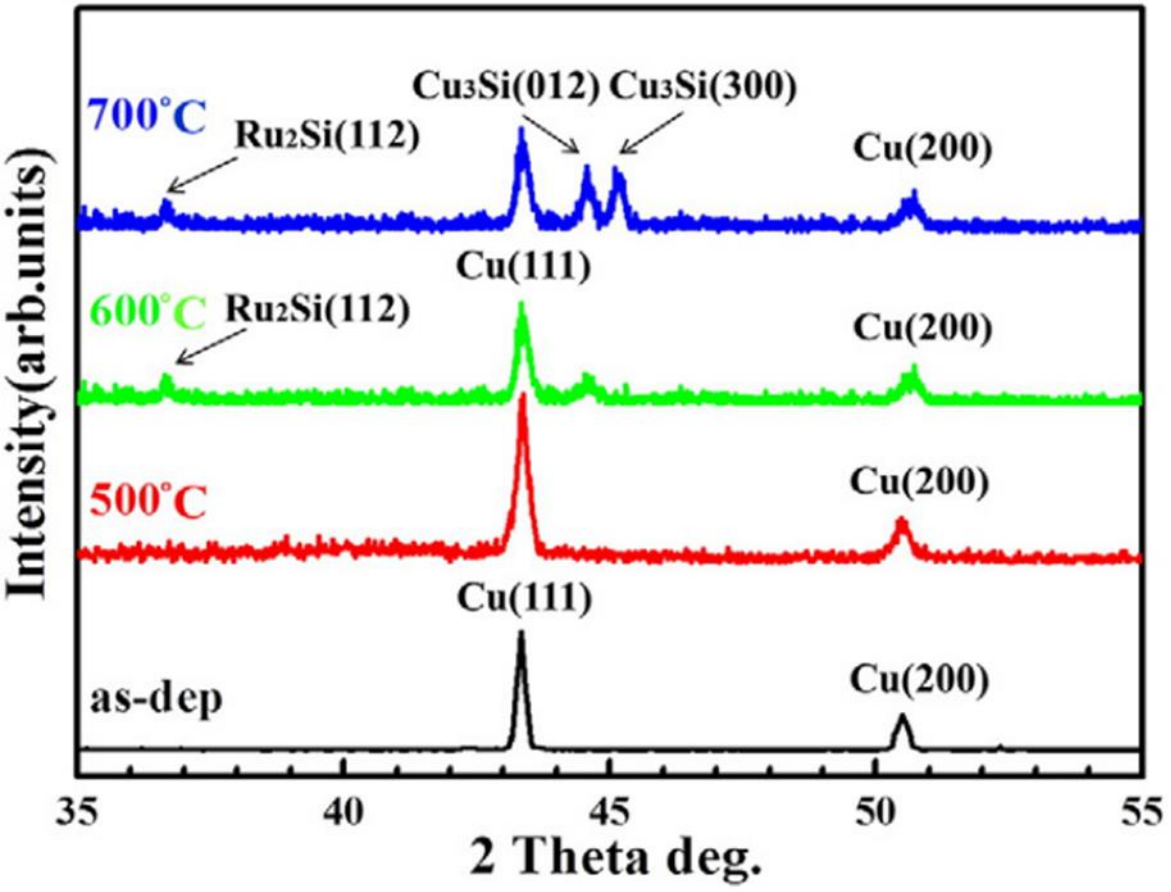

Figure 21 – XRD patterns of Cu/Ru-W(2.5)/Si stack as-deposited and annealed at different temperatures, for 30 min [17].

Damayanti [18] studied Ru-based barrier layers for Cu metallization. The systems encompassed in his work were pure Ru, Ru-N, Ru-W-N and Ru-Ta-N. The addition of N to Ru improved the film microstructure due to the presence of a mixture of amorphous and nanocrystalline phases with 8 to 10 at% of N distributed uniformly. As consequence, N addition slowed down Cu diffusion. However, N diffusion was observed by the author at 275 °C, due to the high thermal instability of Ru-nitrides. To enhance this property, W or Ta were added on Ru-N.

The Ru-W-N films were co-sputtered onto SiO_2/Si substrates in a Cryo Vac sputtering machine, in a mixed Ar and N_2 atmosphere. The Cu layer was also sputtered on Ru-W-N and the samples were annealed at temperatures ranging from 200 to 800 °C for 1 hour, in order to monitor microstructural changes and barrier failure mechanism.

To evaluate the diffusion barrier properties of Ru-W-N, the samples were characterized by XRD and sheet resistance measurements.

Figure 22 shows the XRD spectra for Cu/Ru-W-N/Si stack as-deposited and annealed at temperatures from 400 to 800 °C. For the as-deposited sample as well as the samples annealed at 400, 500 and 600 °, only Cu peaks appears, at 2θ = 43.3º and 2θ = 50.4º. At 700 °C, Ru peaks begin to appear, as result of Ru crystallization, which will facilitate Cu diffusion to the grain boundaries. At 800 °C, the presence of Cu, Ru and W silicides indicate Cu diffusion into Si and barrier failure.

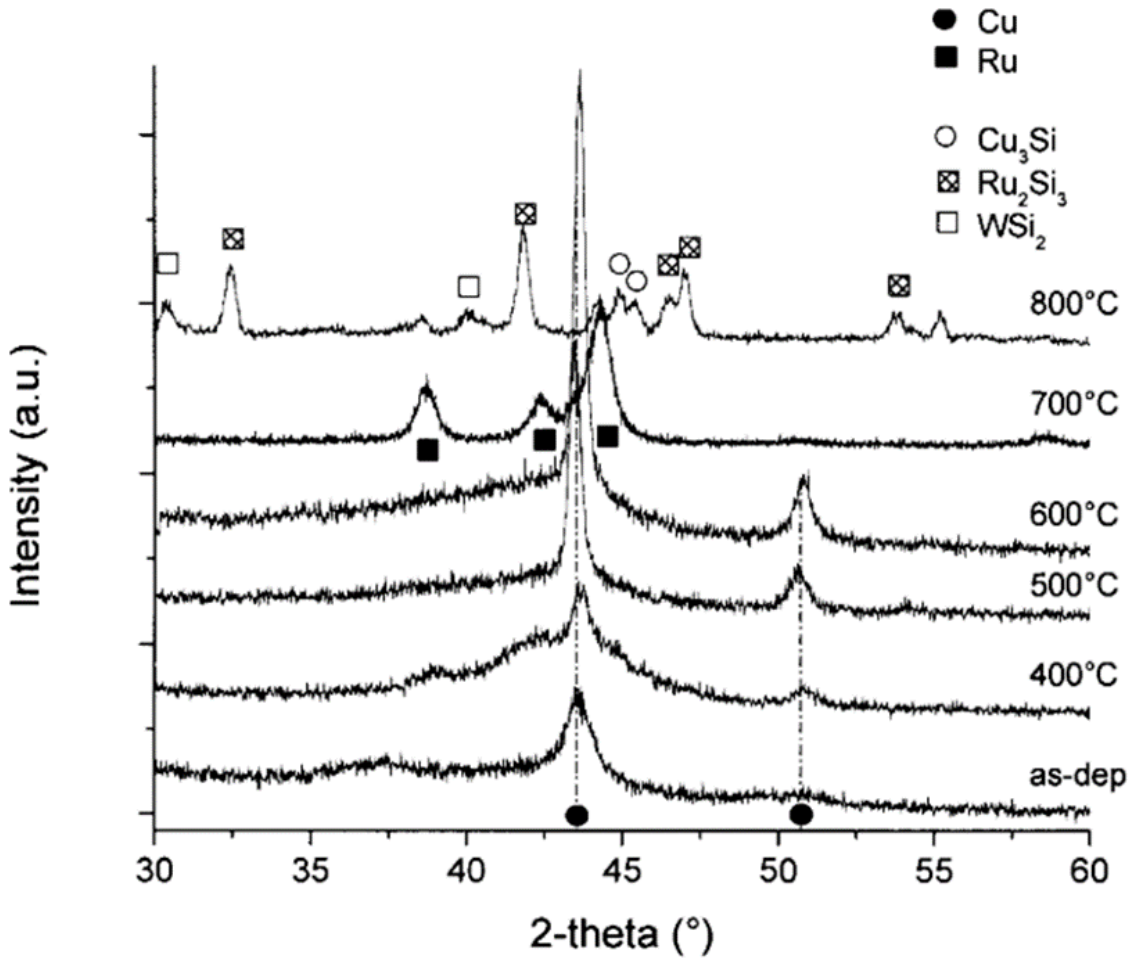

Figure 22 – XRD patterns of Cu/Ru-W-N/SiO_2/Si as-deposited and annealed at different temperatures [18].

For comparison, Table 3 shows the silicide detection temperature for the other Ru-based barrier layers investigated in this work.

Table 3 – Silicide detection temperature, by XRD, of different Ru-based diffusion [18]

	pure Ru	Ru-N	Ru-W-N	Ru-Ta-N
Ru_2Si_3	700 °C	700 °C	800 °C	700 °C
Cu_3Si	800 °C	700 °C	800 °C	700 °C
WSi_2	-	-	800 °C	-
Ta_2Si	-	-	-	800 °C

Figure 23 shows the sheet resistance measurements, for different annealing temperatures, for the Cu/Ru/Si, Cu/Ru-N/Si, Cu/Ru-W-N/Si and Cu/Ru-Ta-N/Si stacks. The decrease in sheet resistance at 400 °C is associated with N release during the annealing. For Cu/Ru-W-N/Si stack, sheet resistance begins to increase at 700 °C, due to Ru crystallization and Cu diffusion, and increases drastically at 800 °C, due to silicide formation which indicates barrier failure. For Cu/Ru/Si, Cu/Ru-N/Si and Cu/Ru-Ta-N/Si, this is observed at 700 °C, meaning that Ru-W-N film was more effective to prevent Cu diffusion. The author attributes Ru-W-N higher thermal stability to the presence of segregated N and/or WN_x at interface, which may delay silicide formation.

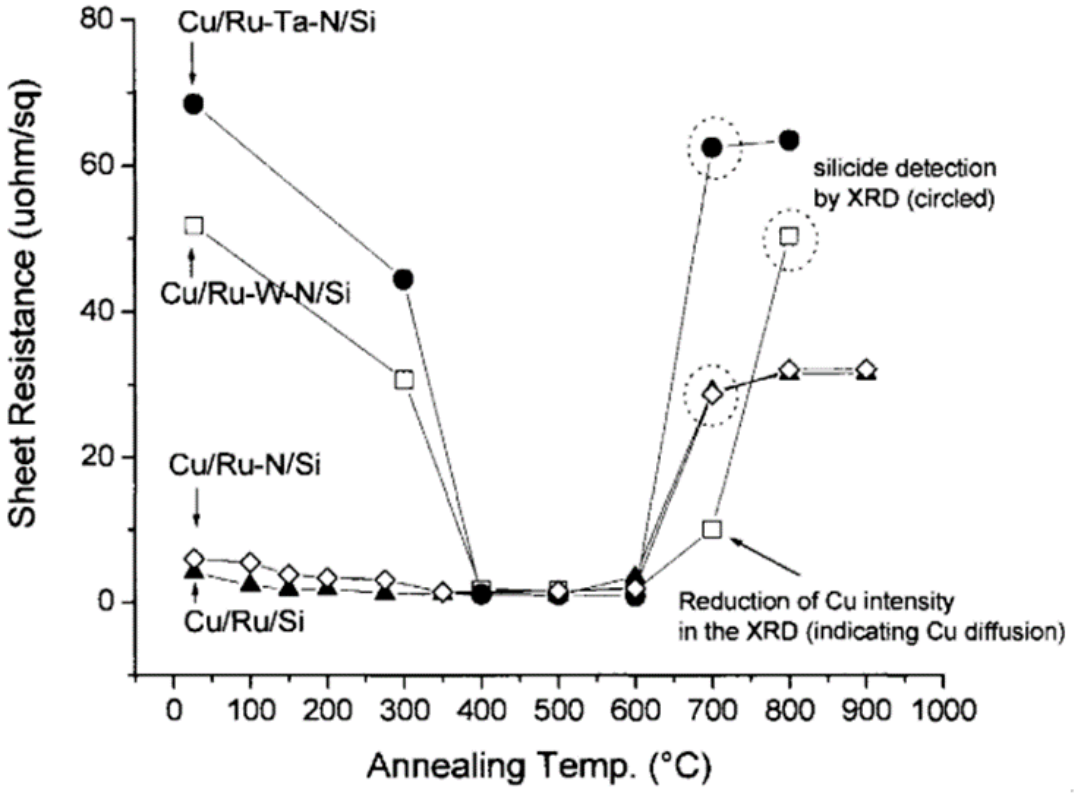

Figure 23 - Sheet resistance of different Ru-based diffusion barrier, for different annealing temperatures [18].

2.2.2 Direct copper plating and wetting ability

Kuo *et al*. [17] also evaluated the direct copper plating and wetting ability of Ru-W films with different W/Ru atomic ratio. Cu was also electroplated on Ta, TaN, Ru and W, for comparison. All the samples were characterized by SEM.

Figure 24 shows SEM images of the nucleation behaviour of EP-Cu on Ta, TaN, Ru and W, for 1 to 60 seconds. Two kinds of nucleation can be seen. First, when Cu is electroplated on Ta, TaN and W, were a non-uniform growth is observed, characterized by the formation of larger Cu clusters, leading to a rough surface morphology. Second, when Cu is electroplated on Ru, the nuclei are small, highly concentrated, and well distributed, characterizing a smooth surface morphology. Despite the better diffusion properties given by the addition of W, from these results, it is possible to conclude that W can have a negative effect on the direct copper plating capability of the Ru-W system.

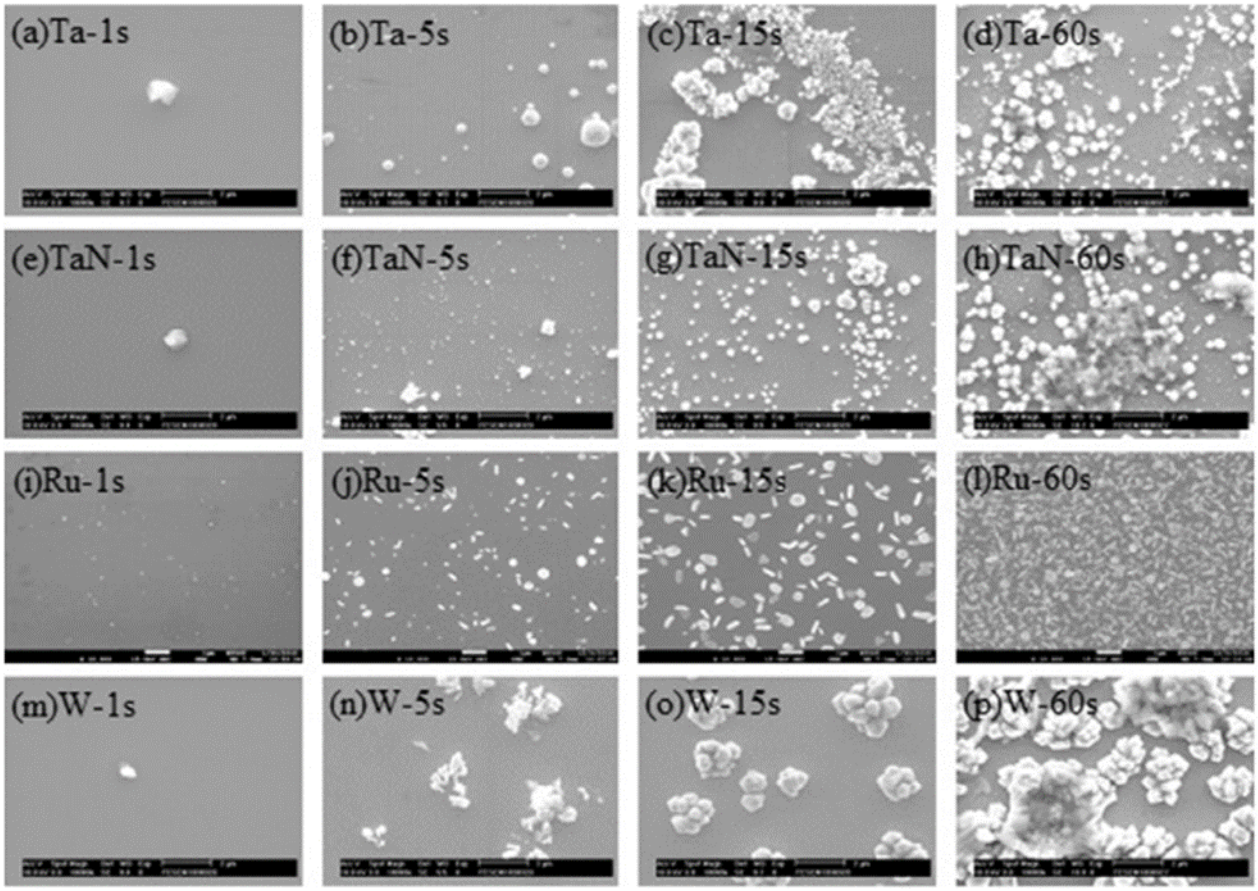

Figure 24 – SEM images of electroplated copper on different substrates with different plating times [17].

Figure 25 shows SEM images of the nucleation behaviour of EP-Cu on Ru-W films with different W/Ru atomic ratios. As expected, samples with higher W content had fewer Cu nuclei, and the formation of larger Cu clusters can be observed.

Table 4 shows the nuclei number and nuclei size for EP-Cu on the different Ru-W substrates. The higher number of Cu nuclei was obtained for the Ru-W(1) substrate, as well as the smallest Cu nuclei.

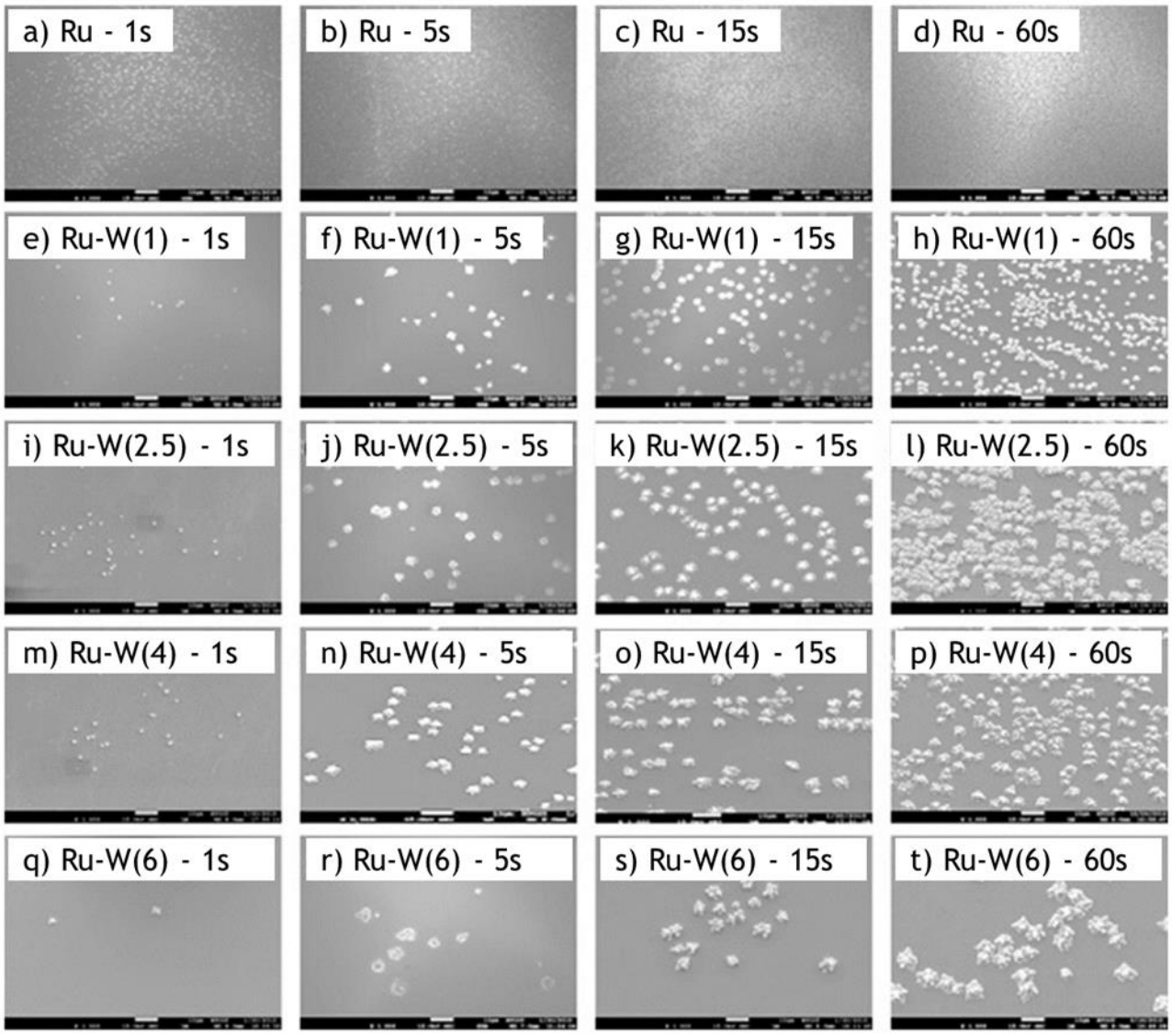

Figure 25 - SEM images of Cu nucleation behaviour on Ru-W films with different W/Ru atomic ratio, for different plating times. Adapted from [15].

Table 4 – Nuclei number and size for EP-Cu on Ru-W substrate with different W/Ru atomic ratio [17]

Substrates	Ru-W(1)	Ru-W(2.5)	Ru-W(4)	Ru-W(6)
Nuclei number	411	269	190	31
Nuclei size (μm)	1.2	3	3.5	5.25

To study the Cu wetting ability of the Ru-W films, the authors submitted the samples to RTA, at different temperatures. Figure 26 shows SEM images of Ru-W films with different W/Ru atomic ratio, after RTA at 400 and 600 °C. At 400 °C, for all samples, the

Cu surface showed small pinholes, with similar dewetting behaviour to Cu/Ru/SiO_2/Si stack (Figure 26a). At 600 °C, the pinholes are larger and increase through enlargement of the W/Ru atomic ratio.

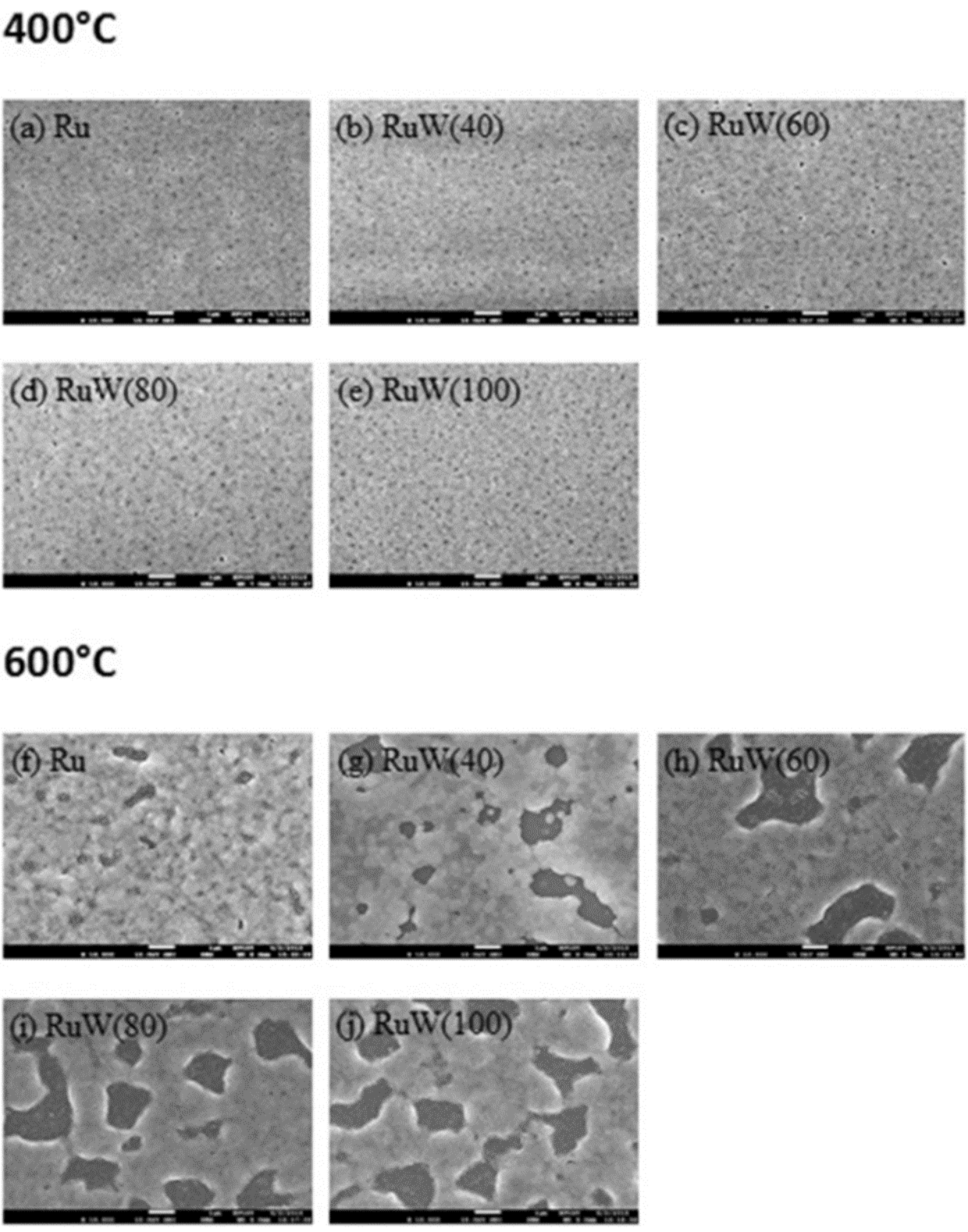

Figure 26 – SEM images of Ru-W films with different W/Ru atomic ratio, after RTA for 400 and 600 °C [17].

The very limited number of studies focusing on the Ru-W as alternative Cu diffusion barrier layers and the scarcity of results related to their direct Cu electrodeposition and Cu wetting ability motived this work which consists of an introductory approach to these underexplored topics.

3. Experimental

3.1 Ru-W thin film deposition

The Ru-W/SiO_2 films were deposited in two steps. First, a ≈100 nm layer of SiO_2 was grown on top of a p-type B-doped Si (100) wafer (Silicon Valley Microelectronics, USA), by plasma enhanced chemical vapour deposition (PECVD) with high RF in a CVD MPX chamber (SPTS Technologies Ltd, UK). Then, the SiO_2/Si wafer was cut in small squares (15 mm x 15 mm) whereon Ru-W films were deposited by DC magnetron sputtering in an ultra-high vacuum sputtering system (Kenosistec, Italy). Ru and W were co-sputtered from their respective targets (99.95%, Testbourne Ltd, UK) for 600 s. A 40 W power bias was applied on the Ru target and a 25 to 100 W was applied on W target, in order to obtain films with different Ru/W ratios. Chamber Ar flux and working pressure were 20 sccm and $6.9x10^{-1}$ Pa, respectively. A contact profilometry instrument (KLA-Tencor, USA) was used to measure Ru-W film thickness.

3.2 Copper electroplating

To investigate the direct copper plating capability of Ru-W, a Cu film was electroplated on top of Ru-W/SiO_2/Si stacks. Figure 27 shows the preparation steps for Cu electroplating.

First, to ensure electrical contact, a piece of Al foil was folded under the sample. Second, a polymeric mask, with 8 mm diameter window, was placed on the substrate surface, to delimitate the deposition area to a circle of 0.5 cm^2. The third step was to place the substrate (cathode) on the deposition cell, a 200 cm^3 poly(methyl methacrylate) container, and to position the counter-electrode (anode), a Cu plate, parallel to the sample. The electrolyte used was an acidic solution containing 0.05 M $CuSO_4 \cdot 5H_2O$ (99.995%, Sigma-Aldrich), 0.05 M H_2SO_4 (Honeywell/Fluka), 1 mM NaCl (Honeywell/Fluka) and 300 ppm poly(ethylene glycol) 600 (Fluka Chemie GmbH) in double-distilled water (4^{th} step) with a pH of ≈ 1.5. The electrodeposition sequences (5^{th} step) were employed using a Gamry potentiostat/galvanostat Interface 1000E (Gamry Instruments, Warminster, PA, USA) with a simple two-electrode cell configuration. The 6^{th} and final step was to remove immediately the samples from the electrolyte, rinsed in double-distillated water and dried with a soft Ar blow.

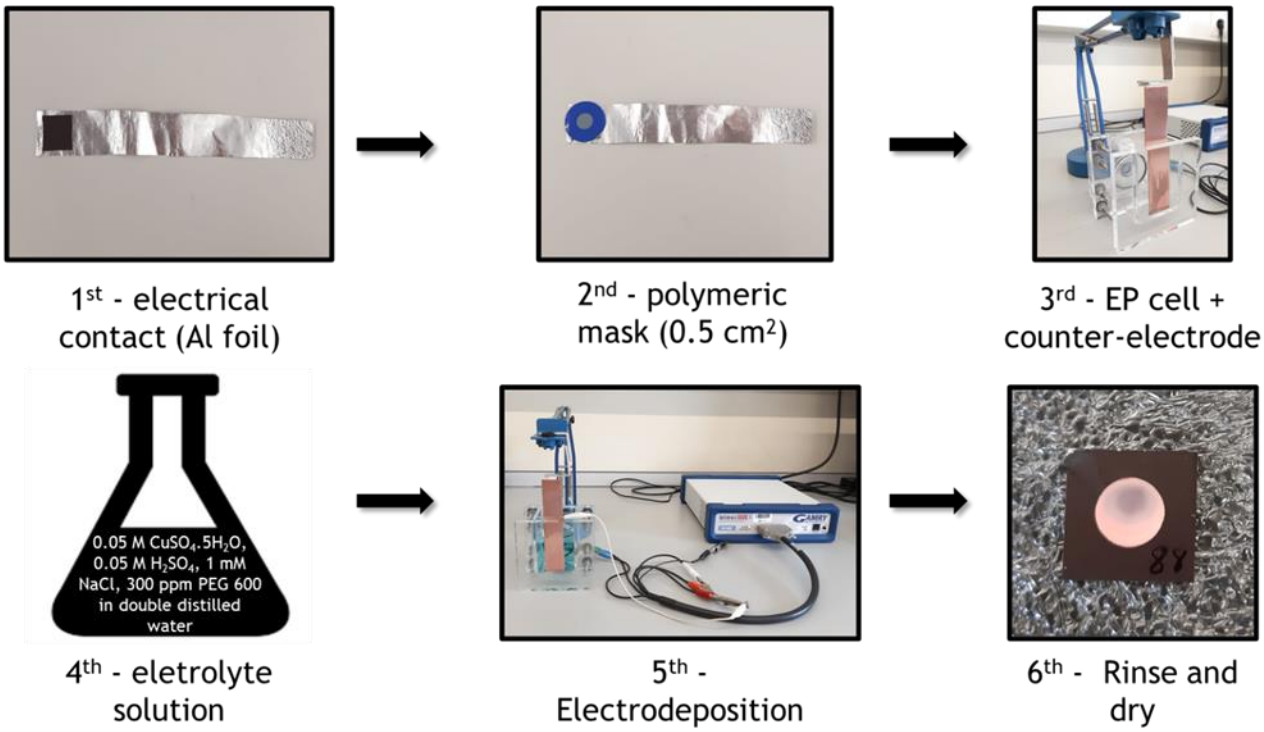

Figure 27 – Cu thin films electrodeposition steps.

3.2.1 Copper electroplating conditions

For advanced copper interconnect metallization, to obtain a uniform, compact and thin EP-Cu film, with a complete substrate coverage is important to achieve conformal fill-up of narrow vias. Therefore, considering an ideal substrate, with infinite number of active sites for Cu nucleation, uniform nuclei growth, and electrodeposition efficiency close to 1, the thickness (h) of the film can be calculated by equation 3, where Q is the total charge transferred per area unit, M is the molecular mass of Cu, ρ is the density of Cu, e is the charge of the electron, O is the oxidation state for Cu ions, and N is the Avogadro's number.

$$h = \frac{QM}{\rho eON} \tag{3}$$

The total charge transferred (Q) can be calculated with equation 4, where J is the average current density and t is the electrodeposition time.

$$Q = J \times t \tag{4}$$

Table 5 summarises different electroplating times (t) and average current densities (J) explored in this work, to comprise a Q of 300 mC and produce, in ideal conditions, an EP-Cu film of ≈ 110 nm. The application of a continuous cathodic current (DC) and the alternation between cathodic and anodic pulse (pulse-reverse current (PRC)) were both used in this work. In Table 5, j_c and j_a are the cathodic and anodic current densities, and t_c and t_a are the cathodic and anodic current times.

Table 5 – Process conditions for Cu electrodeposition on Ru-W

Sample ID	J mA·cm^{-2}	t s	Q mC	j_c mA·cm^{-2}	j_a mA·cm^{-2}	t_c ms	t_a ms
DC-2	2	150	300	-	-	-	-
DC-5	5	60	300	-	-	-	-
DC-10	10	30	300	-	-	-	-
PRC-5	3	100	300	5	5	20	5
PRC-10	6	50	300	10	10	20	5
PRC-20	12	25	300	20	20	20	5

For PRC samples, J values were obtained with equation 5.

$$J_{PRC} = \frac{(j_c \times t_c) - (j_a \times t_a)}{t_c + t_a} \quad (5)$$

3.3 Cu thin film deposition

In order to investigate Cu wetting ability of Ru-W thin films, Cu thin films were deposited on top of Ru-W/SiO_2/Si and Ta/SiO_2/Si stacks by DC magnetron sputtering in an ultra-high vacuum sputtering system (Kenosistec, Italy). A power bias of 40 W was applied at the Cu target (99.95%, Testbourne Ltd, UK) for 900 s and 1800 s, to obtain films with two different thicknesses. Chamber Ar flux and working pressure were 20 sccm and 6.9x10^{-1} Pa, respectively. A contact profilometry instrument (KLA-Tencor, Milpitas, CA, USA) was used to measure Cu films thickness.

3.4 Annealing treatment

The PVD-Cu/Ru-W/SiO_2/Si and PVD-Cu/Ta/SiO_2/Si stacks were submitted to annealing treatment at 600, 650 and 700 °C for 60 minutes, in a tubular furnace (Termolab, Portugal) (Figure 28) with a heating and cooling rate of 5 ºC/min and a working pressure of ≈ 1 x 10^{-3} Pa.

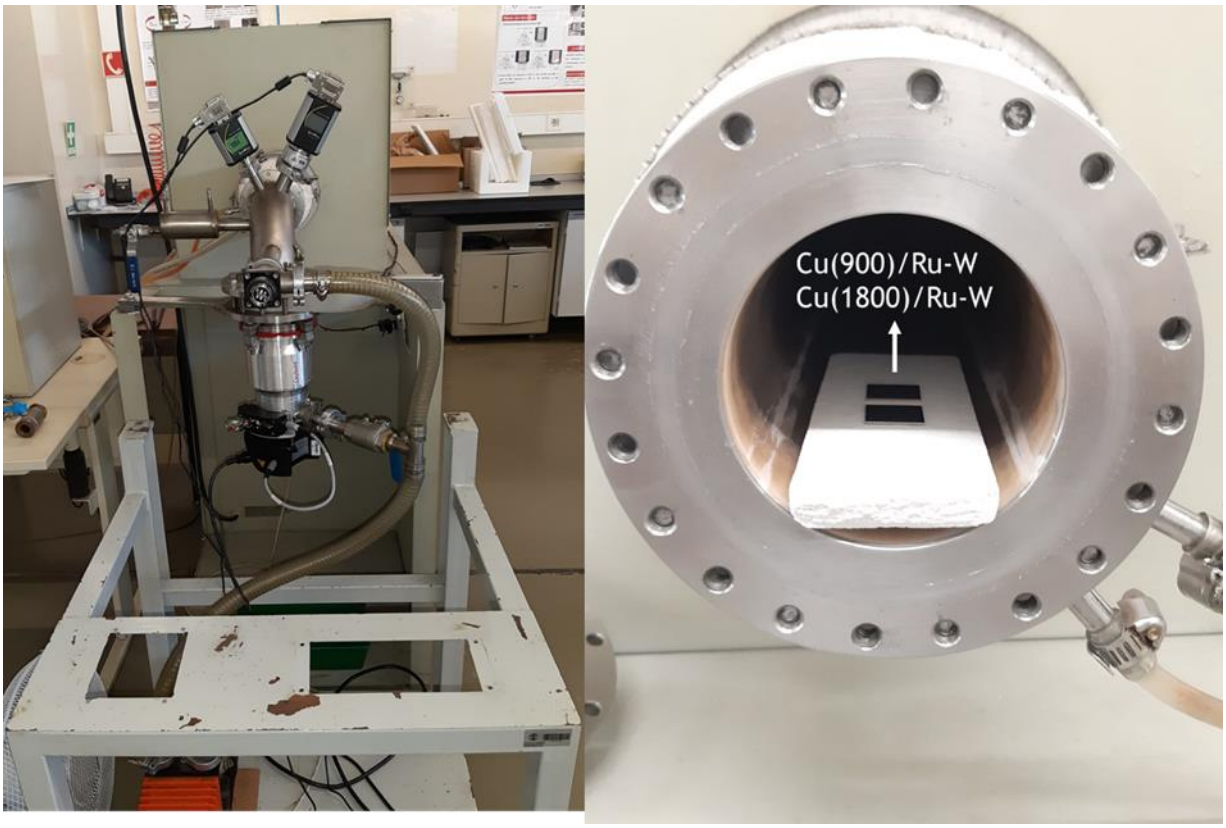

Figure 28 – Tubular furnace where annealing treatments were carried.

3.5 Structural and chemical characterization

The surface of the PVD Ru-W/SiO_2/Si thin film, as-sputtered, was observed by SEM (FEI Quanta 400FEG ESEM), and the chemical composition was estimated by EDS (EDAX Genesis X4M). Ru-W film structure was determined by grazing incidence X-ray diffraction (GIXRD) at an angle of 1.5º, using Cu Kα radiation (λ = 1.54060 Å), and a step of 0.04 $^{\circ}\cdot s^{-1}$. The Cu/Ru-W/SiO_2/Si stacks were analysed by SEM and digital microscopy (Leica DVM6). The Cu-substrate interface cross-section was prepared by focused ion-beam (FIB) milling (FEI Helios 450S).

4. Results and discussion

4.1 Direct copper plating capability of Ru-W thin films

As aforementioned, different compositions of Ru-W thin films (≈15 nm) were produced by varying the power bias applied to the W target, while maintaining the power bias to Ru target at 40 W. Figure 29 shows the correlation between Ru/W atomic ratio and the power bias applied to the W target, where the Ru/W atomic ratios were estimated by EDS with a 15 keV electron beam and collection time of 200 s.

For this work, Ru-W films with equimolar composition (Ru/W ≈ 1) were selected for direct Cu electroplating, which was achieved through a power bias of 30 W applied at the W target. This decision was made based on results obtained by Kuo *et al.* [17] where the highest Cu nucleation density was observed for a Ru/W atomic ratio equal to 1 (Figure 25), as well as to compare with the results obtained for Co-W by Santos, R. F. et al. [15].

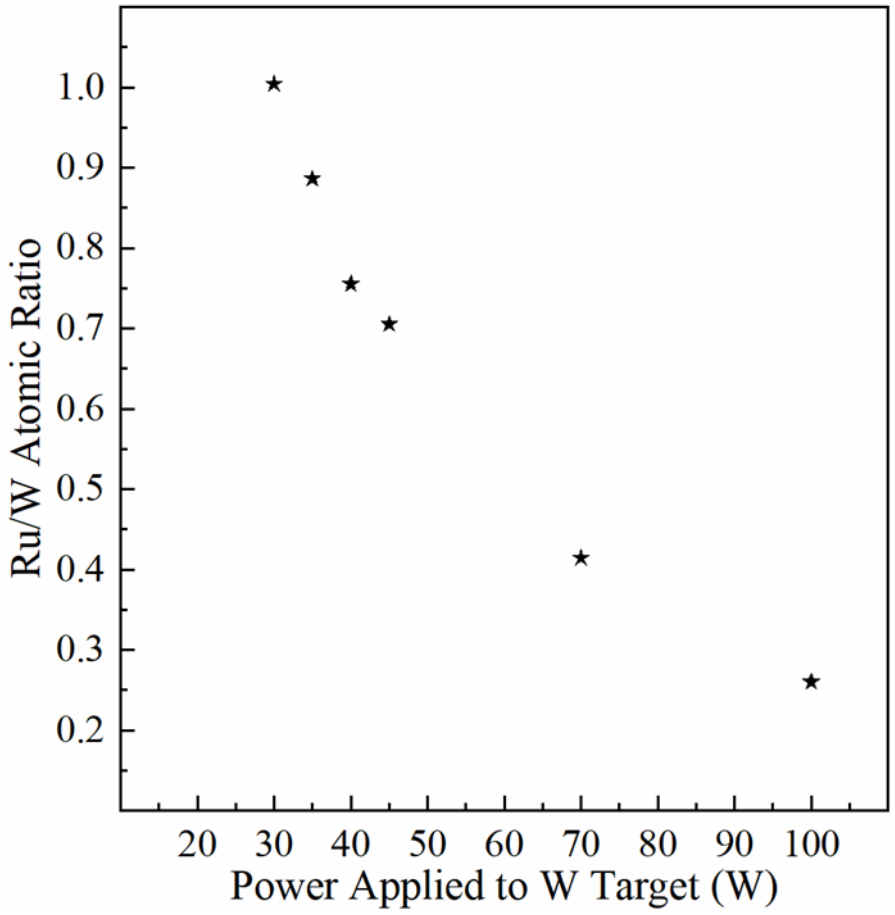

Figure 29 – Ru/W atomic ratio as function of the power applied to W target.

Figure 30a shows the X ray diffractogram of Ru-W, which suggests an amorphous structure, due to the absence of metallic Ru and/or W diffraction peaks. This is an important feature to exhibit as an effective diffusion barrier, which has been previously identified in both Co-W and Ru-W [13, 14, 17, 18]. A smooth and continuous surface can be seen in Figure 30b.

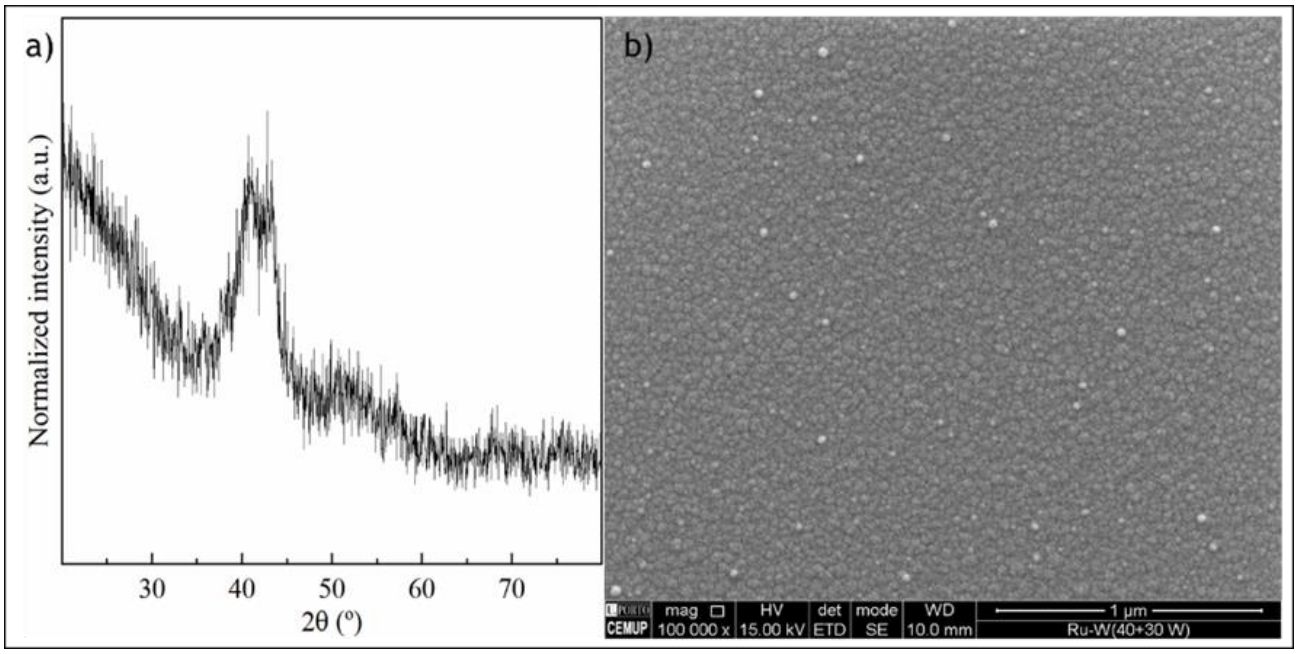

Figure 30 – (a) X-ray diffractogram of Ru/W film, as-sputtered and (b) SEM image of the surface.

Digital microscopy images of the surface of Cu/Ru-W films, as-deposited, can be seen in Figure 31. The electrochemical reactions of Cu electrodeposition for the substrate (cathode) and the counter-electrode (anode) are presented on equation 6.

$$Cu^{2+} + 2e^{-} \rightarrow Cu \quad \text{(cathodic)}$$
$$Cu \rightarrow Cu^{2+} + 2e^{-} \quad \text{(anodic)} \qquad (6)$$

For low values of *J*, 2 and 3 mA·cm^{-2}, the surface coverage is poor, forming a ring-like deposit, as shown in Figure 31a and Figure 31d. A complete surface coverage was achieved for average current density of 5 mA·cm^{-2} and above (Figure 31b,c,e,f). However, EP-Cu film thickness is not uniform across the surface of Ru-W substrate, which is indicated by the differences in colour tonality from the centre, which appears to be thinner, to the edges of the deposit. For average current densities of 5 mA·cm^{-2} and above, it is possible to observe regions where H_2 bubbles were formed, as indicated by the arrows in Figure 31b,c,e,f, due to the co-reduction of H^+ into H^0, which is an undesirable effect that lowers the electroplating efficiency. A few dragging marks can be seen in the images, which resulted from accidental mishandling of the specimens.

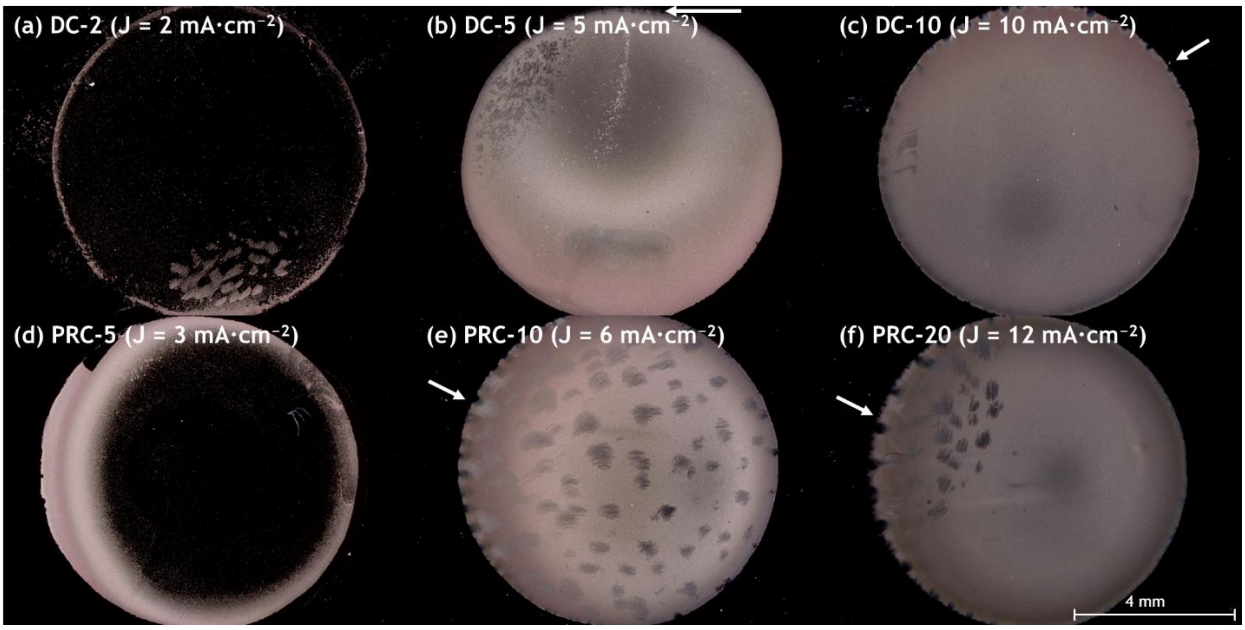

Figure 31 - Digital microscopy images of as-deposited Cu/Ru-W with J values of (a) 2, (b) 5 and (c) 10 mA·cm^{-2}, for DC, and (d) 3, (e)6 and (f) 12 mA·cm^{-2}, for PRC.

Figure 32 shows SEM images of Cu/Ru-W films, at the central (thinner) regions. For all samples a heterogeneous growth of Cu crystals can be observed. For samples with *J* values of 3 mA·cm^{-2} and lower (Figure 32a,d), the nucleation density is very low, where most of the transferred charge is used to grow the small number of nuclei that forms. For average current densities of 5 mA·cm^{-2} and higher (Figure 32b,c,e,f), it is possible to see Cu crystals with different shapes and sizes, that nucleate and grow on the Ru-W substrate. It can be noted that despite the small difference in J values between DC-5 and PRC-10, the average size of Cu nuclei in PCR-10 appears to be much smaller than in DC-5. Still, the way the current is applied, PCR or DC, leads to a great difference in substrate coverage, in DC-5 and PRC-5.

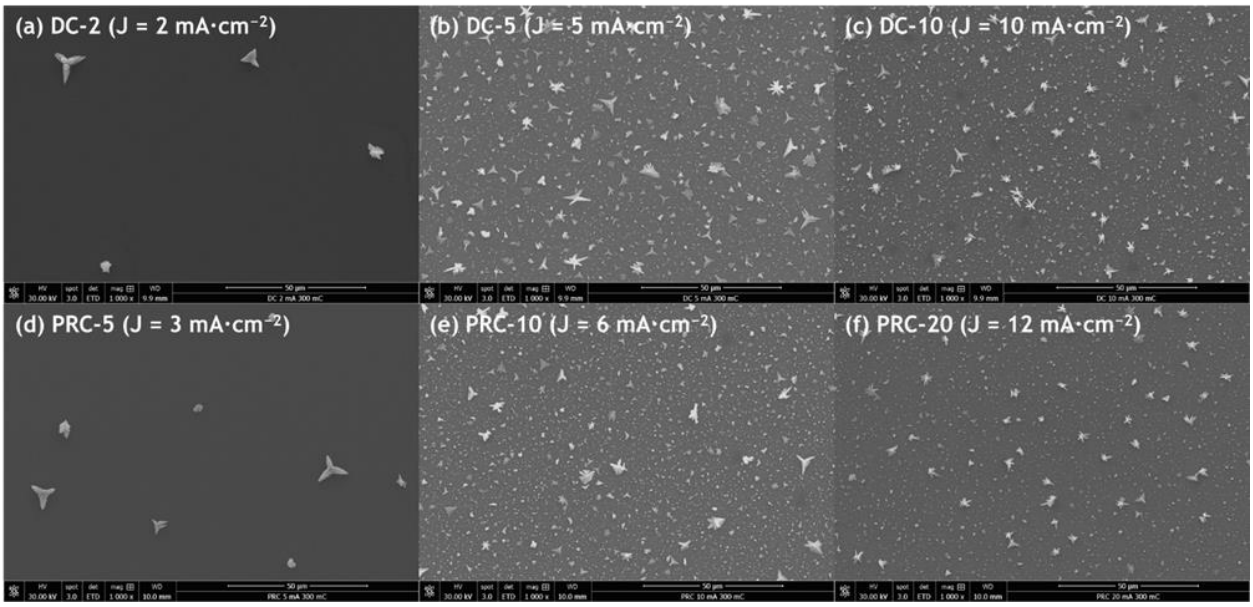

Figure 32 - SEM images of central (thinner) regions of as-deposited Cu/Ru-W with J values of (a) 2, (b) 5 and (c) 10 mA·cm^{-2}, for DC, and (d) 3, (e) 6 and (f) 12 mA·cm^{-2}, for PRC.

Figure 33 shows SEM images of the same regions of Figure 32, at higher magnification. A good surface coverage is observed for samples with *J* values of 5 mA·cm^{-2} and above, where the area between large Cu crystals is covered with a uniform and continuous film. For these electroplating conditions, a high density of nuclei form in the early stages of electrodeposition, following a lateral growth, towards the direction perpendicular to the Ru-W substrate. The Cu nuclei grow in all directions, at similar rate, until they become particles with approximately the same size, that impinge on each other and stop growing. This will result in an uniform and continuous film, covering most of the Ru-W substrate. However, as can be seen in Figure 33, some of the Cu nuclei presented a much higher growing rate, resulting in large Cu crystals, with a size of approximately 1 to 3 μm. These crystals have a different growth mechanism, following specific crystallographic directions, resulting in different faceted/polygonal shapes. This effect (Figure 33f) is not desirable, since it impedes an uniform growth across the surface as well as prevents Cu nuclei to form and grow in the surrounding area, resulting in a non-continuous Cu film with large polygonal crystals surrounded by uncovered substrate. The growth mechanism herein proposed is illustrated in Figure 34.

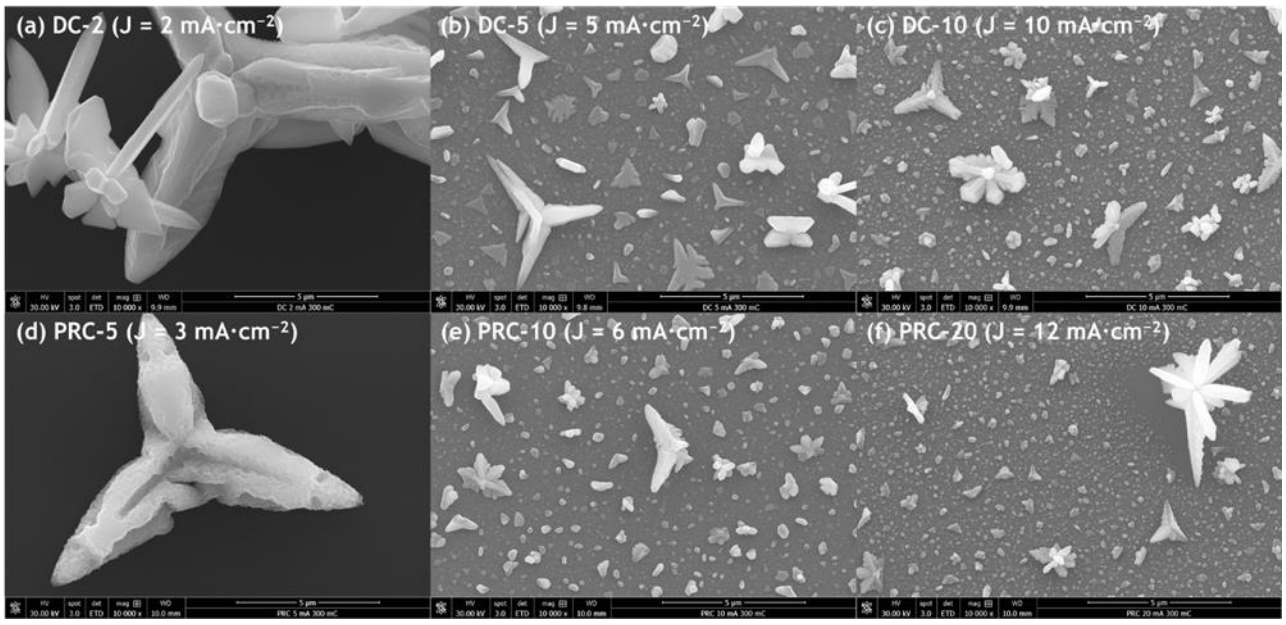

Figure 33 – SEM images of the same regions of Figure 32, at higher magnification.

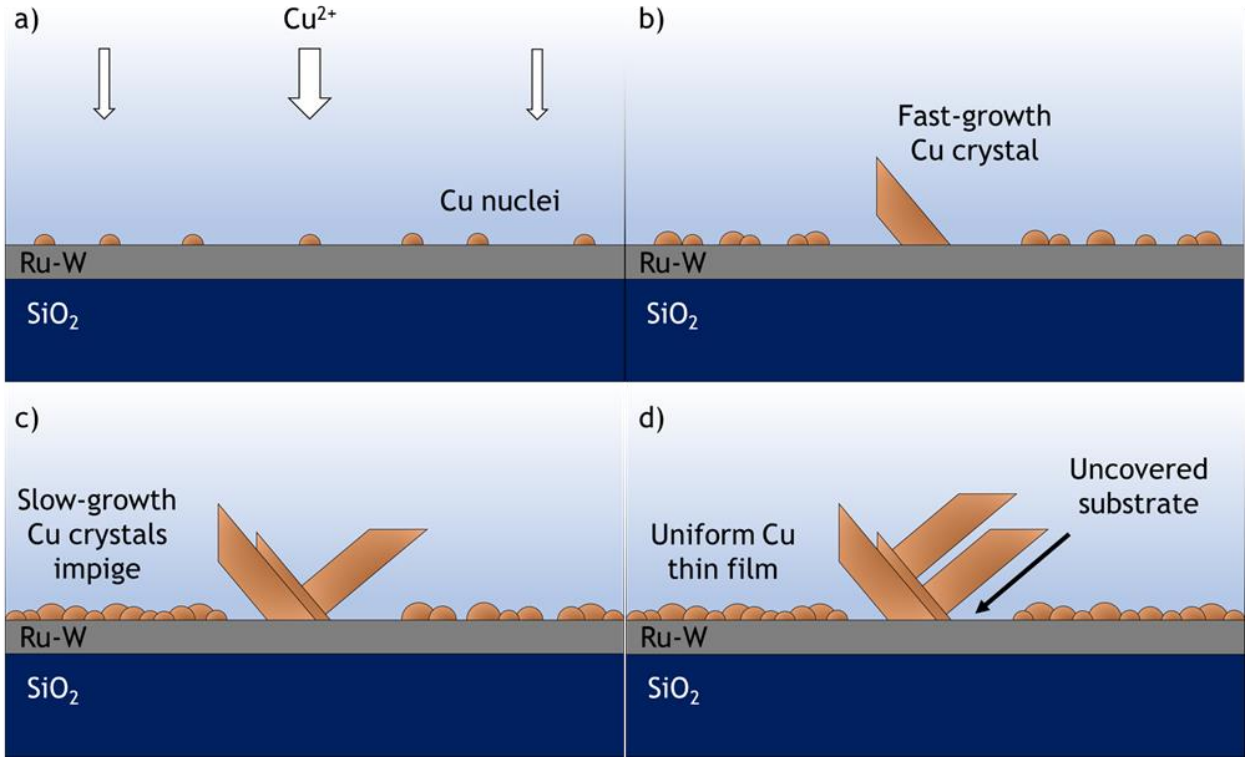

Figure 34 - Early stages of Cu film formation on Ru-W. (a) First nuclei appear (b) where a few grow with a faster rate, consuming more Cu^{2+}. (c) Slow-growing Cu crystals impinge on each other and (d) form a continuous Cu film, while fast-growing crystals impede substrate coverage underneath them.

This can be seen more clearly in Figure 35a, where around large particles, Ru-W substrate is uncovered. SEM imagens obtained by backscattered electrons (BSE), such as Figure 35b, emphasize this effect, by showing darker regions in the surroundings of large Cu crystals, as indicated by the black arrows. With the absence of Cu, the signal comes only from the substrate, which is composed by Ru, W and Si. Despite Ru and W being heavier elements than Cu, which means that the region around the large particles should appear brighter in BSE images, the Ru-W films are very thin (≈ 15 nm). Therefore, most of the signal is coming from Si, a much lighter element than Cu, Ru and W, resulting in a darker region.

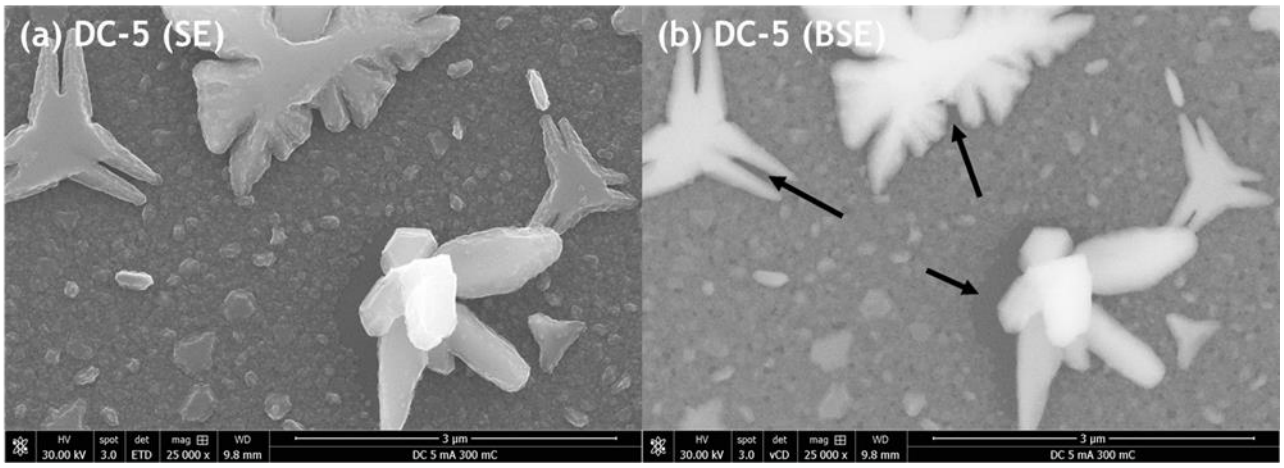

Figure 35 – SEM image of as-deposited DC-5 sample obtained by (a) secondary (SE) and (b) backscattered electrons (BSE).

Figure 36 shows SEM images of as-deposited Cu/Ru-W films, at higher average current densities (DC-10 and PRC-10). As observed, increasing *J* value from 5 to 10 mA·cm^{-2} in DC does not improve substrate coverage, where darker regions around large Cu crystals still can be seen in Figure 36a. However, the average size of large particles is reduced, being a beneficial effect, since the surroundings of this particles have poor substrate coverage.

For PCR-10, in Figure 36b, the surface seems to be smoother than in DC-10, even though the number of large particles does not appear to change. In the pulse-reverse current deposition, the cathodic process of ion reduction is alternated with an anodic (reverse) pulse that oxides back the less attached Cu atoms while helping the solid-liquid interface to replenish with Cu^{2+}. This process conditions allow Cu film to grow more uniformly, hindering the formation of no coverage zones around growing particles.

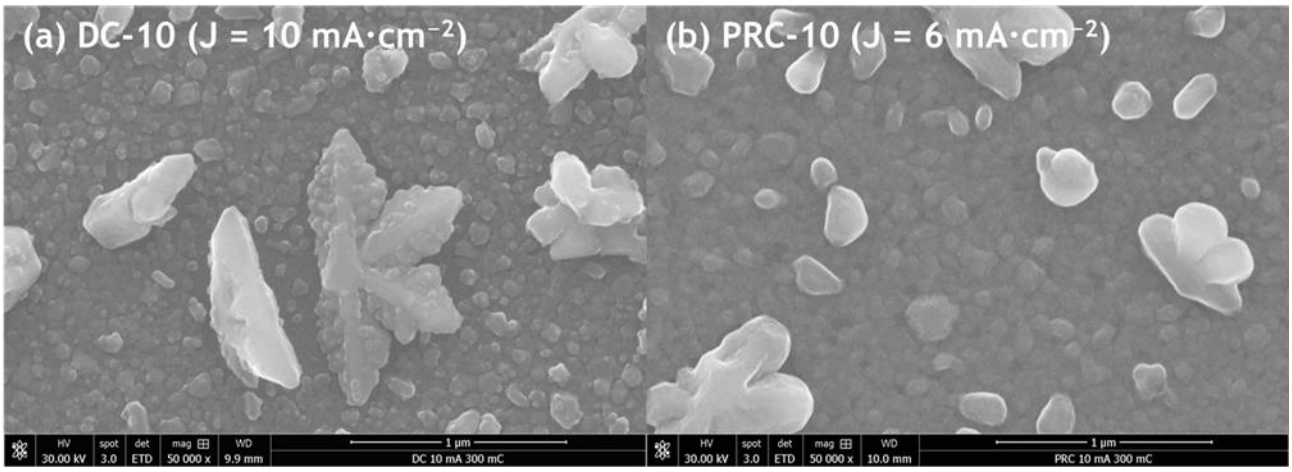

Figure 36 – SEM imagens of as-deposited Cu/Ru-W (a) DC-10 and (b) PRC-10 samples.

A comparison between DC-5 and PRC-10 is shown in Figure 37. Despite the similar average current densities, 5 and 6 mA·cm^{-2}, respectively, PRC-10 appears to have smaller average particle size. This was confirmed through the measurement of particles for both samples.

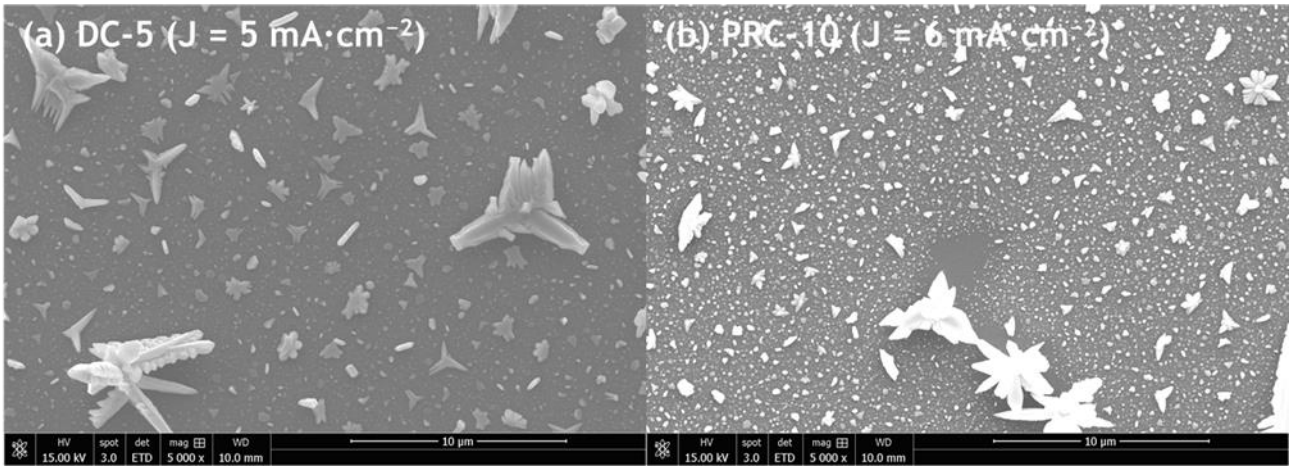

Figure 37 - SEM imagens of as-deposited Cu/Ru-W (a) DC-5 and (b) PRC-10 samples.

The methodology used is shown in Figure 38, where a circle with a minimum diameter, equivalent of 800 nm, was used to delimitate the particles. For both samples, all the

particles with 800 nm and more were measured, totalizing 71 particles for DC-5 and 58 for PRC-10. As expected, the majority of PRC-10 particles are small, having less than 2 µm with an average particle size of 1.31 µm. DC-5 however, presents larger particles, with a few ones with more than 7 µm and an average particle size of 1.57 µm (Figure 39). Therefore, the transferred charge used to form and grow large particles in DC-5 is being used to form small particles in larger quantity in PRC-10.

On top of that, in PRC-10, the hydrogen evolution becomes important, in comparison to what happens in DC-10, which reduces the electrodeposition efficiency. In this case, hydrogen formation and Cu^{2+} reduction compete, resulting in a decrease of the effective current.

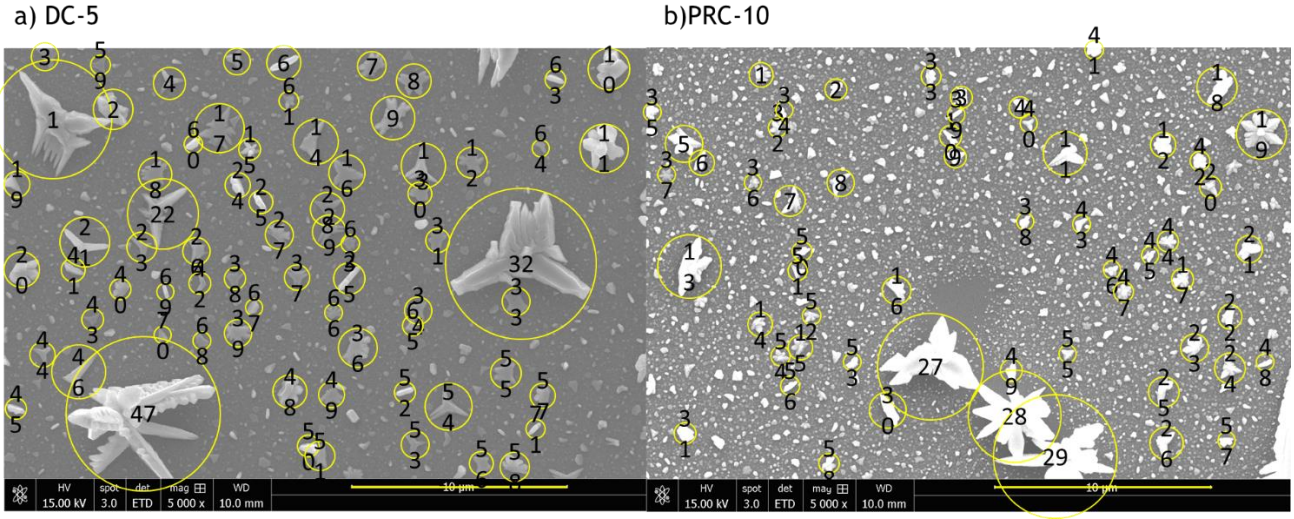

Figure 38 -Measurement method used to measure particles size for samples (a) DC-5 and (b) PRC-10.

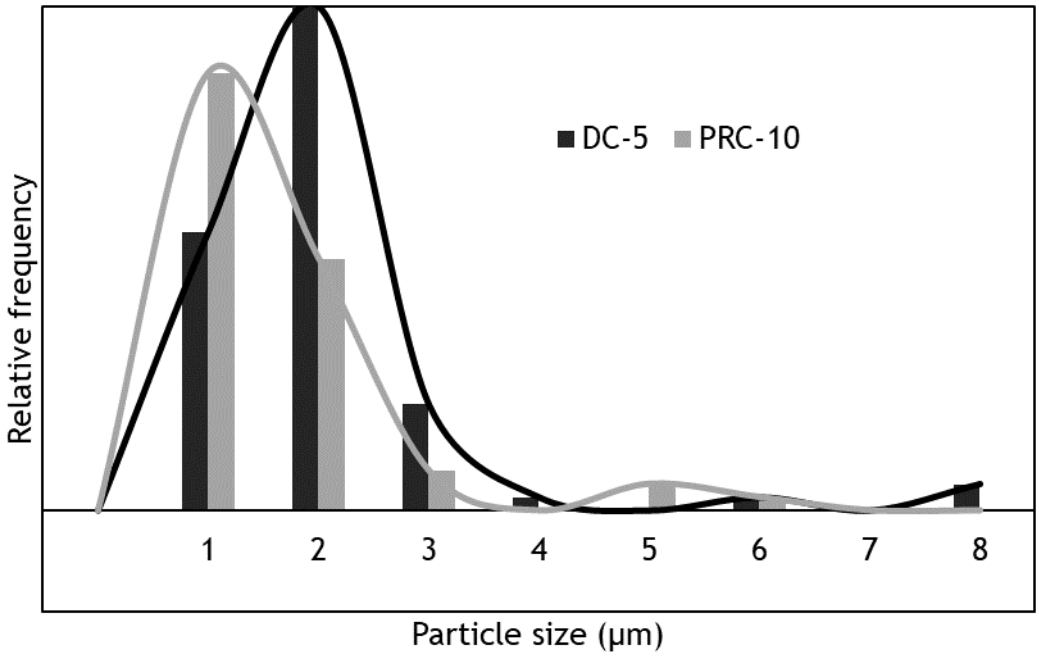

Figure 39 – Relative number of particles as function of particle size for samples DC-5 and PRC-10.

Aiming at substrate coverage improvement, new samples were produced, namely DC-2, DC-5 and DC-10, with tree times the initial deposition time, totalizing 900 mC of charge transferred. Digital microscopy and respectively SEM images of these samples are shown in Figure 40.

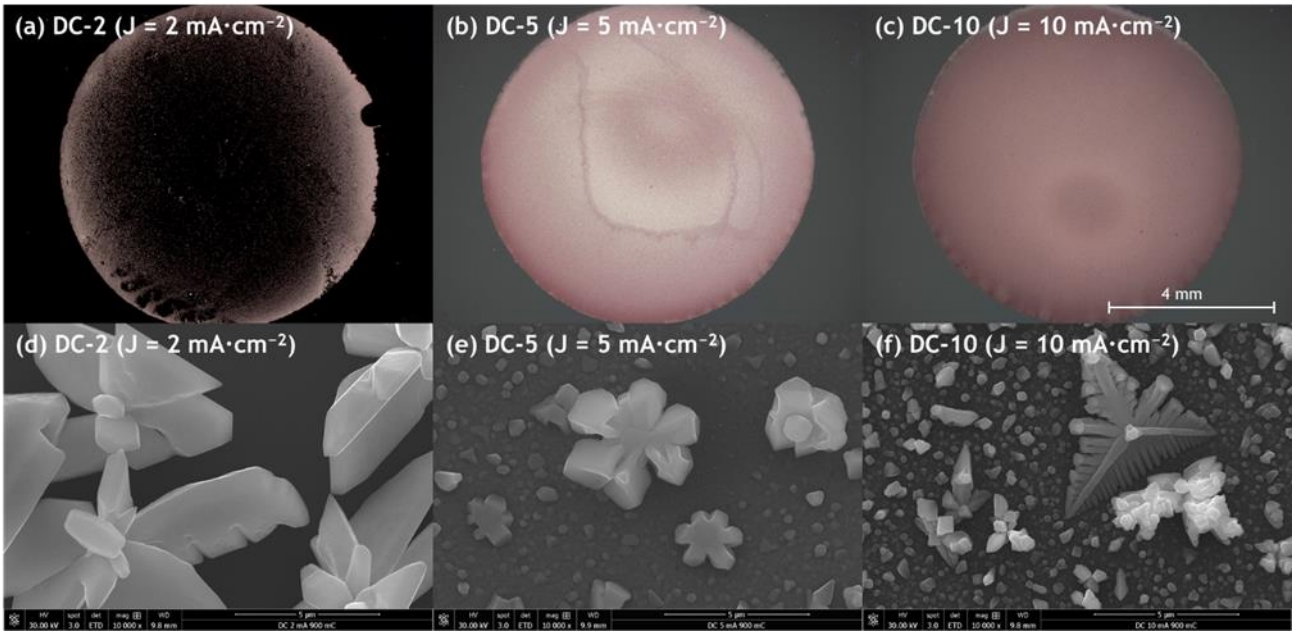

Figure 40 - Digital microscopy images of as-deposited Cu/Ru-W with 900 mC of charge transferred for samples (a) DC-2, (b) DC-5 and (c) DC-10 and respectively SEM imagens.

Even with triple charge transferred, at 2 mA·cm^{-2}, a poor surface coverage can be seen (Figure 40a). The SEM image in Figure 40d shows that the 900 mC are consumed by growing the existing Cu particles, while the nucleation density does not increase. For average current densities of 5 and 10 mA·cm^{-2} and above, complete surface coverage is achieved (Figure 40b, c) and improves around larger Cu crystals (Figure 40e,f). Despite the majority of the Cu film growth being in the normal direction, some lateral expansion of Cu particles is observed. This helps reduce the gaps between these particles and the thinner Cu film areas. However, some portions of the substrate remain uncovered.

At ideal conditions (*i.e.* uniform Cu film growth and electrodeposition efficiency close to 1) these Cu films should be 330 nm thick, according to equation 1 and considering Q = 900 mc. Figure 41 shows images of samples DC-5 and DC-10, for 900 mC, prepared by FIB. Thickness measurements from Figure 41 are shown in Table 6.

Table 6 - Thickness measurements from samples DC-5 and DC-10 after FIB milling

Sample ID	Thickness - *h*
DC-5	≈ 240 - 270 nm
DC-10	≈ 80 – 150 nm

For both samples, the difference between measured and calculated thickness can be attributed to the non-uniform distribution of Cu mass across the surface of Ru-W

substrate. Still, the co-reduction of hydrogen, that consumes part of the charge transferred also affects the efficiency of the process, which increases the difference between measured and calculated thickness. This effect is more intense at 10 mA·cm^{-2}, which, in part, explain the lower thickness of DC-10 sample.

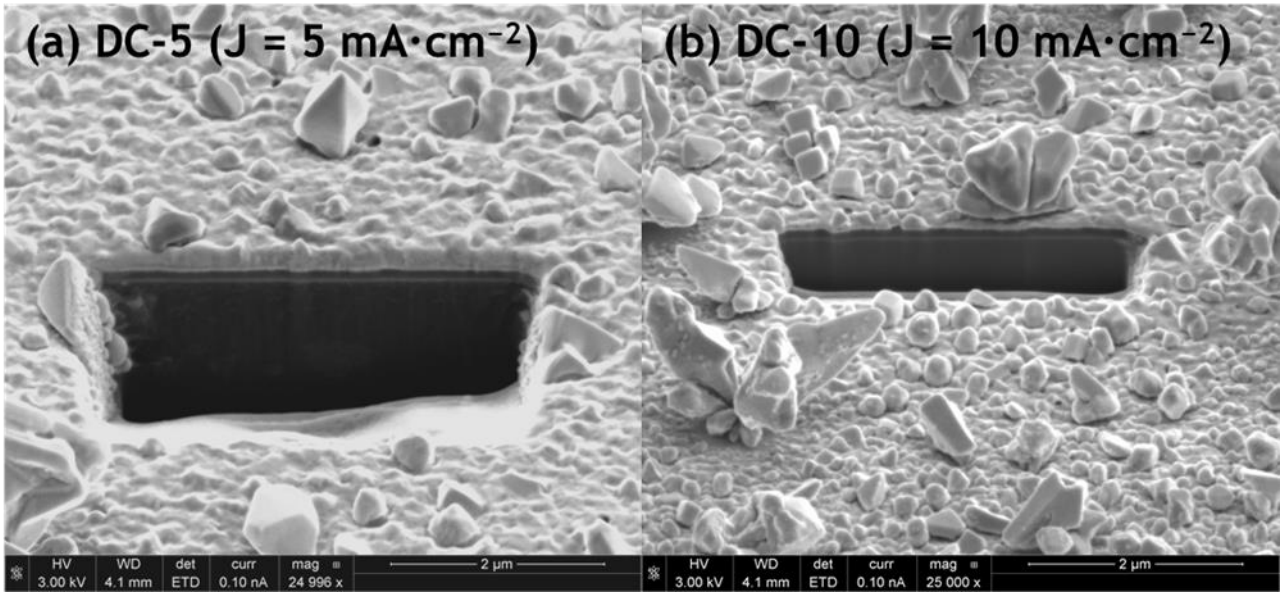

Figure 41 - FIB-cut samples of as-deposited Cu/Ru-W films at (a) 5 and (b) 10 mA·cm^{-2}, observed at 40° tilt angle.

The Cu electroplating results on Ru-W substrate obtained can be compared with the study previously developed on the project USECoIN [15]. The dissolution phenomenon was not observed for Ru-W films, where, as exception of the few surrounding areas of large crystals, a complete surface coverage was achieved for DC of 5 mA·cm^{-2} and above, as shown in Figure 31. Therefore, even though both systems, Ru-W and Co-W, are directly electroplatable from copper acidic solution, Ru-W presented better performance at low pH (<2).

4.2 Copper wetting ability of Ru-W thin films

To be an alternative for Ta/TaN, the direct copper plating capability is an important feature that novel diffusion barriers should exhibit. However, the adhesion to Cu is a fundamental property. A strong adhesion between Cu and Ru-W is not only fundamental to reduce the effects of electromigration but also essential to resist the fabrication process flow which include heat treatments.

The dewetting phenomena, of a film deposited on a substrate, is directly related to film thickness and temperature, having as the driving force the minimisation of the system's interfacial energy. If the interfacial energy between the substrate and the vacuum (or other medium), γ_s, is higher than the sum of the interfacial energy between the film and the substrate, γ_i, and the interfacial energy between the film and the vacuum (or other medium), γ_f, ($\gamma_s > \gamma_i + \gamma_f$) the film is stable and does not dewet [20]. To investigate Cu wetting ability of Ru-W thin films, PVD-Cu/Ru-W/SiO_2/Si stacks were submitted to annealing treatments. The Cu films were deposited with two different

thicknesses, by varying the PVD deposition time (900 and 1800 seconds). A comparison was made by submitting Cu/Ta/SiO_2/Si stacks to the same annealing treatments.

Figure 42 shows SEM images of Cu/Ru-W/SiO_2/Si and Cu/Ta/SiO_2/Si stacks, in the as-deposited condition and after annealing treatment for 60 min at 600, 650 and 700 ºC, with Cu film thickness of ≈ 35 nm. As observed, the Cu film surface is mostly uniform and continuous on both Ru-W and Ta substrates, in as-deposited condition (Figure 42a,b). In spite of the thin nature of the Cu film, at 600 ºC the grain growth is clear in both stacks (Figure 42c,d). It is also noteworthy the appearance of pinholes on Cu films' surface. Similar defects were identified by Kuo et al. [17], as mentioned in chapter 2.2.2., and have been associated with the beginning of the dewetting phenomena of Cu thin films on a Ru-W substrate at 400 ºC, acting as precursors for film cracking and agglomeration, observed at 600 ºC. However, in this case, the number and size of pinholes remain sensibly the same up to temperatures of 700 ºC (Figure 42e,g) in the Cu/Ru-W stack. No evidence of Cu film cracking and agglomeration was found in this range of temperatures, being difficult to attribute their appearance exclusively to dewetting phenomena. It is possible that such pinholes were pre-existent with a smaller size in the as-deposited condition, although not easily seen in Figure 42a,b. Pinholes are common defects in films fabricated by PVD, especially in lower thicknesses, caused by small discontinuities/gaps on the substrate's surface [21]. It is possible that the degree of roughness on Ru-W and Ta surfaces may have facilitated the formation of pinholes in the Cu films therein sputtered. As the temperature increases and atomic diffusion rearranges the as-deposited Cu microstructure, pinholes become more visible, with a circular/ellipse shape given by the reduction in interfacial energy.

Figure 43 shows SEM images of both stacks, Cu/Ru-W/SiO_2/Si and Cu/Ta/SiO_2/Si after annealing at the same temperatures, with Cu thickness of ≈ 70 nm. In these films, pinholes are frankly smaller in number, which can be attributed to higher film thickness, but are easier to see. Also, grain growth is even more evident, consequence of a thicker Cu film. Thicker films should be less susceptible to dewetting which, in this case, holds true. Since that at 35 nm no significant dewetting is present (Figure 42c-h), it should not be expected at 70 nm, under the same temperature ranges (Figure 43c-h).

Figure 43d shows what appears to be Cu film disruption on Ta, at 600 ºC, across considerably large areas, that is easily distinguishable from pinholes, also present at that temperature. However, it does not seem reasonable to attribute this to dewetting at 600 ºC since it was not observed at higher temperatures. It is unclear what is this disruption on the surface of the Cu/Ta/SiO_2/Si stack annealed at 600 ºC, but the SEM images suggest a change in the topography around those regions. It is also unclear the appearance of bright spots along grain boundaries on Cu/Ru-W/SiO_2/Si stack surface (Figure 43g) which could be attributed to localised oxidation during annealing at high temperature, preferably on grain boundaries, assuming residual oxygen contamination inside the tubular furnace. Nevertheless, this cannot not explain why Cu/Ta/SiO_2/Si stack does not display the same granular structure (Figure 43h) since both stacks were placed closely inside the furnace and annealed at the same time.

Dewetting phenomena of Cu/Ta, Cu/Co-W, and Cu/Ru-W reported in [12, 17] display a characteristic Cu film disruption morphology, characterised by film cracking, agglomeration, and island formation, at temperatures up to 600 ºC, by RTA. Such morphology contrasts to what is observed in Figure 42 and Figure 43 where the Cu film remains continuous, except for the formation of pinholes. It is reasonable to admit that the thermal stability of Cu films on Ru-W is comparable to their Cu/Ta equivalents, offering resistance to dewetting up to 700 ºC under the annealing conditions (i.e. vacuum and slow heating/cooling rate, 60 min. stage), which differ from RTA reported in the literature. The annealing parameters may play a decisive role on the dewetting behaviour of Cu thin films which increases the difficulty of comparing results that were obtained under different conditions and equipment.

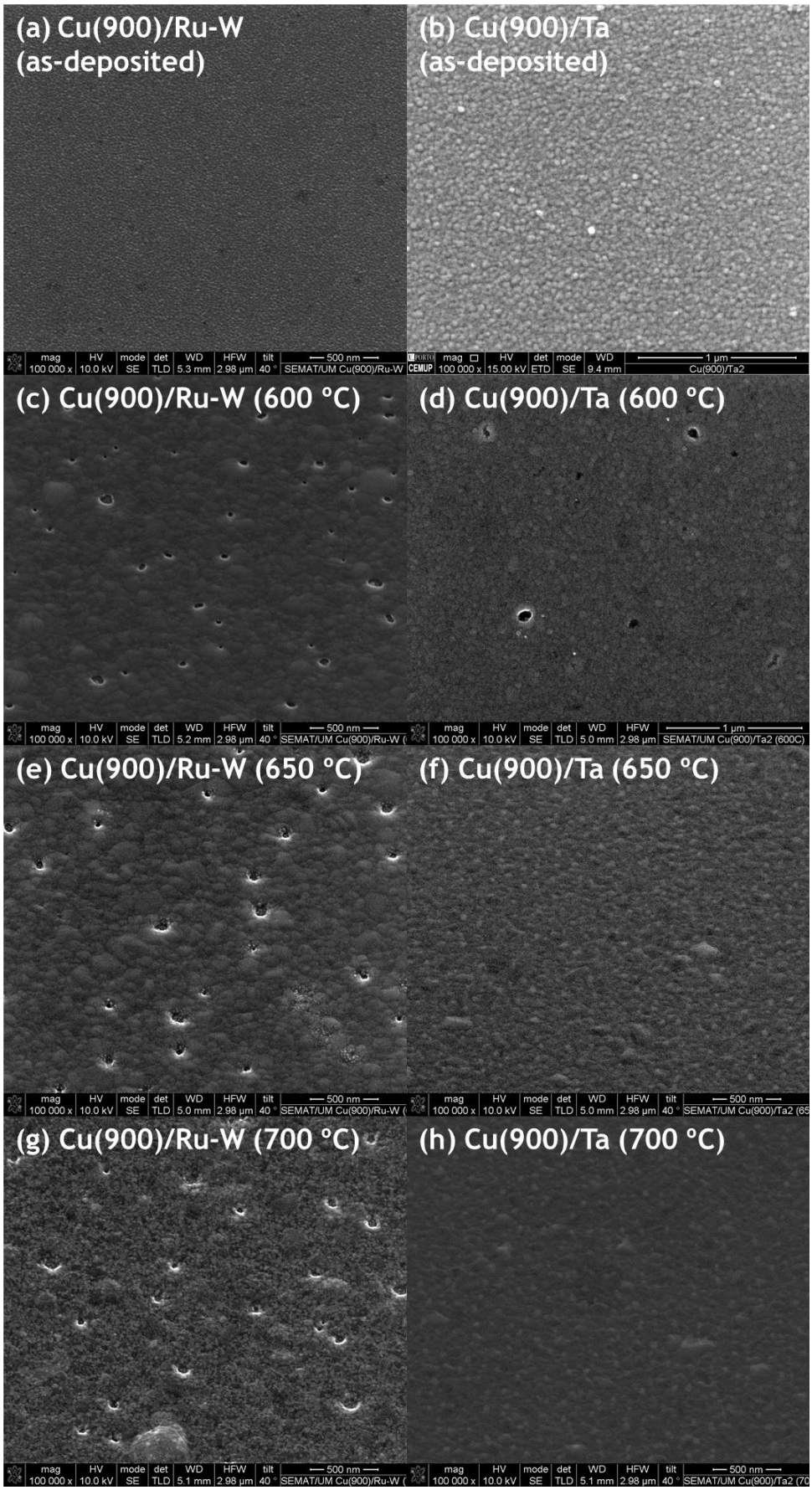

Figure 42 – SEM imagens of Cu(900)/Ru-W/SiO_2/Si and Cu(900)/Ta/SiO_2/Si stacks (a,b) as-deposited and after annealing treatment for 60 min at (c,d) 600, (e,f) 650 and (g,h) 700 ºC, respectively.

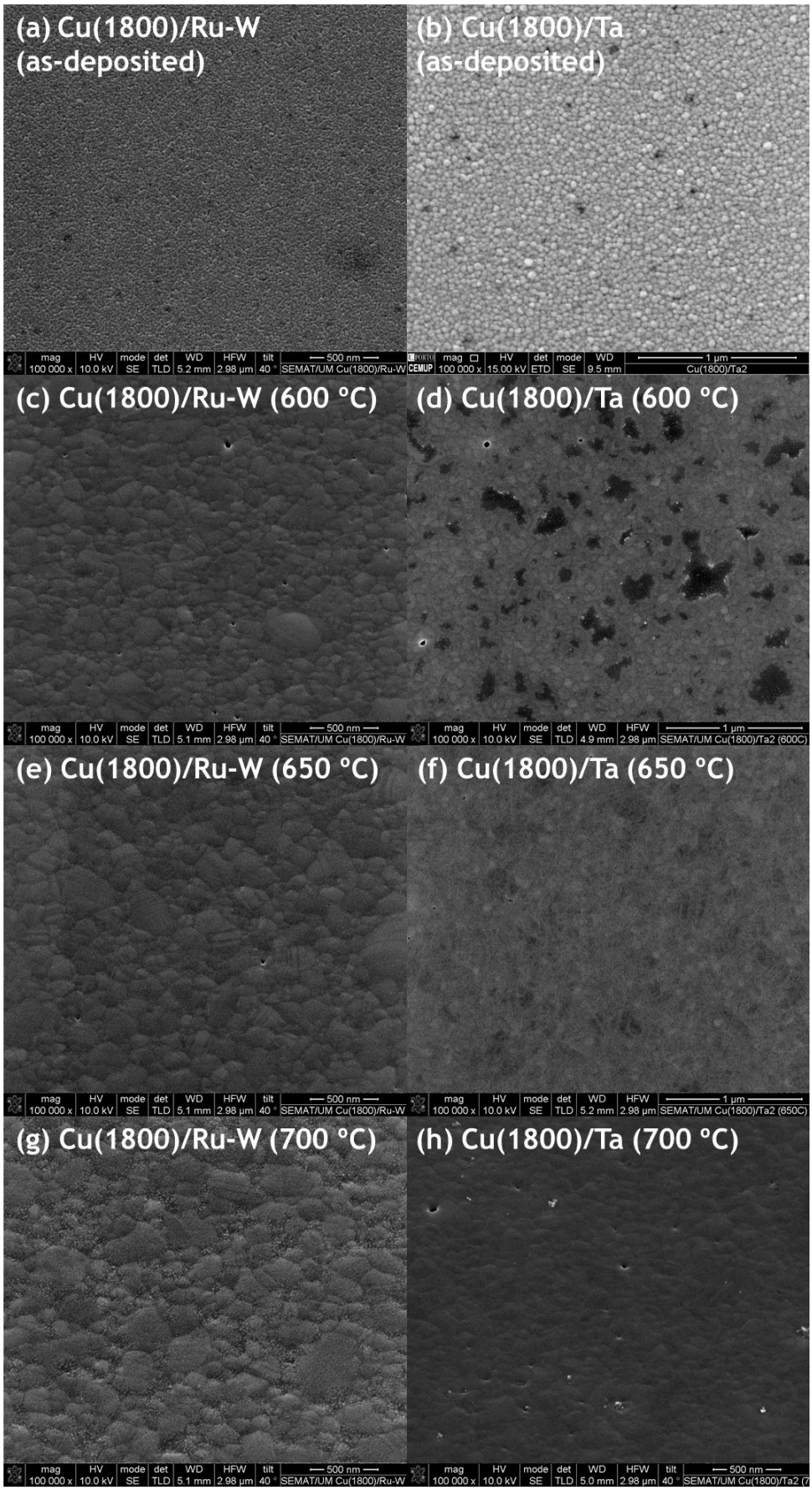

Figure 43 - SEM imagens of Cu(1800)/Ru-W/SiO_2/Si and Cu(1800)/Ta/SiO_2/Si stacks (a,b) as-deposited and after annealing treatment for 60 min at (c,d) 600, (e,f) 650 and (g,h) 700 ºC, respectively.

5. Conclusions

Direct (seedless) Cu electroplating was performed on top of Ru-W thin films with Ru/W atomic ratio close to 1, as candidates to replace Ta/TaN as diffusion barriers layers for advanced Cu metallization. The electrodeposition process was carried out using a Cu sulphate acidic electrolyte (pH < 2). From this investigation, it is possible to conclude that Ru-W diffusion barriers are directly electroplatable from copper sulphate solution. A continuous Cu film was obtained for DC densities of 5 $mA \cdot cm^{-2}$ and above, where small currents originate low nucleation rate. However, the formation of large particles, with fast growing rate, was observed, hindering the substrate coverage underneath them. Even for higher DC density, 10 $mA \cdot cm^{-2}$, a complete surface coverage was not achieved, due the presence of the large particles. Pulse-reverse current (j = 10 $mA \cdot cm^{-2}$) can help reduce particle size, possibly improving substrate coverage, since the uncovered areas are the large particles surroundings. However, the hydrogen evolution becomes relevant for average current densities of 6 $mA \cdot cm^{-2}$ and above, as observed in this work, which will compete with Cu deposition for the transferred charge, lowering the process efficiency. Despite the large particle formation, for application as Cu interconnects, Cu is electroplated on very small areas, so it is probably that the surface coverage achieved in this work would be enough to form a continuous film on the vias/lines. Nevertheless, in order to improve the direct Cu plating capability of Ru-W films, investigate different methods could be necessary, namely electrodeposition through modified electrolytes, under ultrasonic agitation, under different temperatures, among others.

The adhesion between Cu and Ru-W was investigated by submitting PVD-Cu/Ru-W/SiO_2/Si stacks with two different thicknesses (35 and 70 nm) to annealing treatment at different temperatures. The thinner Cu films presented the formation of pinholes at 600 ºC, which is associated in the literature as the beginning of the dewetting phenomena. However, in this work dewetting was not observed, even for 700 ºC. Therefore, the pinhole formation could be attributed to PVD process defects, due to the lower thickness. For the Cu film with 70 nm, only a few pinholes appear. As expected, no dewetting was observed. In conclusion, for the annealing conditions investigated in this work, the thermal stability of Cu films on Ru-W substrate is comparable with Cu on Ta-TaN, showing dewetting resistance up to 700 ºC.

References

1. Colinge, J.-P. and J.C. Greer, *1.1 Moore's Law*, in *Nanowire Transistors - Physics of Devices and Materials in One Dimension*. 2016, Cambridge University Press.
2. Apple. *Apple unveils all-new iPad Air with A14 Bionic, Apple's most advanced chip*. 2020 [cited 2021 February, 24]; Available from: https://www.apple.com/pt/newsroom/2020/09/apple-unveils-all-new-ipad-air-with-a14-bionic-apples-most-advanced-chip/.
3. Gupta, T., *Copper interconnect technology*. 2010: Springer Science & Business Media.
4. Jones, A.C. and M.L. Hitchman, *9.2.1 Diffusion Barrier Layers*, in *Chemical Vapour Deposition - Precursors, Processes and Applications*. 2009, Royal Society of Chemistry.
5. Baklanov, M., P.S. Ho, and E. Zschech, *Advanced interconnects for ULSI technology*. 2012: John Wiley & Sons.
6. Basak, T.K., *4.10.3 Wafer Test*, in *Electrical Engineering Materials*. 2012, New Academic Science.
7. Lindroos, V., et al., *39.1.4.3 Copper Electroplating*, in *Handbook of Silicon Based MEMS Materials and Technologies*. 2010, Elsevier.
8. Hübner, R.J.L.-e.M.S.R., *Advanced Ta-based diffusion barriers for Cu interconnects*. 2008: p. 183.
9. Starosvetsky, D., N. Sezin, and Y. Ein-Eli, *Seedless copper electroplating on Ta from a "single" electrolytic bath*. Electrochimica Acta, 2010. **55**(5): p. 1656-1663.
10. Shacham-Diamand, Y., et al., *Advanced nanoscale ULSI interconnects: fundamentals and applications*. 2009: Springer.
11. Babu, S., *2.2.5 Diffusion Barrier/Cu Seed Stack Layers*, in *Advances in Chemical Mechanical Planarization (CMP)*. 2016, Elsevier.
12. Su, Y.-H., et al., *Effect of tungsten incorporation in cobalt tungsten alloys as seedless diffusion barrier materials*. Microelectronic Engineering, 2017. **171**: p. 25-30.
13. Shimizu, H., K. Sakoda, and Y. Shimogaki, *CVD of cobalt–tungsten alloy film as a novel copper diffusion barrier*. Microelectronic Engineering, 2013. **106**: p. 91-95.
14. Shimizu, H., et al., *Atomic layer deposited Co (W) film as a single-layered barrier/liner for next-generation Cu-interconnects*. 2012. **51**(5S): p. 05EB02.
15. Santos, R.F., et al., *Seedless Cu Electroplating on Co-W Thin Films in Low pH Electrolyte: Early Stages of Formation*. 2021. **11**(8): p. 1914.
16. Bernasconi, R. and L. Magagnin, *Review-ruthenium as diffusion barrier layer in electronic interconnects: current literature with a focus on electrochemical deposition methods*. Journal of the Electrochemical Society, 2019. **166**(1): p. 3219-25.
17. Kuo, T.-C., et al., *A study on the plating and wetting ability of ruthenium-tungsten multi-layers for advanced Cu metallization*. Microelectronic Engineering, 2016. **162**: p. 27-33.

18. Damayanti, M., *Study of Ruthenium-based Barrier Layer for Copper Metallization*. 2009, Nanyang Technological University.
19. Greenslit, D., et al., *Development of plasma-enhanced atomic layer deposition grown Ru–WCN mixed phase films for nanoscale diffusion barrier and copper direct-plate applications*. 2009. **27**(2): p. 631-636.
20. Thompson, C.V.J.A.R.o.M.R., *Solid-state dewetting of thin films*. 2012. **42**: p. 399-434.
21. Panjan, P., et al., *Review of growth defects in thin films prepared by PVD techniques*. 2020. **10**(5): p. 447.